JPET Fast Forward. Published on January 8, 2019 as DOI: 10.1124/jpet.118.253708
This article has not been copyedited and formatted. The final version may differ from this version.

Manuscript title

Brain distribution and active efflux of three panRAF inhibitors: considerations in the treatment of melanoma brain metastases

Authors and affiliations

Gautham Gampa, Minjee Kim, Afroz S. Mohammad, Karen E. Parrish, Ann C. Mladek, Jann N. Sarkaria and William F. Elmquist

Brain Barriers Research Center, Department of Pharmaceutics, College of Pharmacy, University of Minnesota, Minneapolis, Minnesota, USA (GG, MK, ASM, KEP, WFE)

Radiation Oncology, Mayo Clinic, Rochester, Minnesota, USA (ACM, JNS)

Running title

Brain delivery of panRAF inhibitors

Corresponding author

William F. Elmquist

Professor

Department of Pharmaceutics

University of Minnesota

308 Harvard Street SE

Minneapolis MN 55455

E-mail. elmqu011@umn.edu

Tel. +1(612) 625-0097

Fax. +1(612) 626-2125

Numbers

Number of text pages: 31

Number of tables: 7

Number of figures: 10

Number of references: 55

Number of words in abstract: 250

Number of words in introduction: 749 (excluding in-text citations)

Number of words in discussion: 1482 (excluding in-text citations)

Abbreviations

AUC, area under the curve

BBB, blood-brain barrier

Bcrp, breast cancer resistance protein (Abcg2)

BSA, bovine serum albumin

CL, clearance

Cmax, maximum drug concentration

CNS, central nervous system

DA, distribution advantage

fu, unbound (free) fraction

F, bioavailability

FVB, friend leukemia virus strain B

IC_{50}, half-maximal inhibitory concentration

Kp, brain-to-plasma ratio

Kp,uu, unbound (free) brain-to-plasma ratio/ unbound partition coefficient

LC-MS/MS, liquid chromatography tandem mass spectroscopy

MAPK, mitogen-activated protein kinase

MBM, melanoma brain metastases

MDCKII, Madin-Darby canine kidney II

NCA, non-compartmental analysis

PBS, phosphate buffered saline

OS, overall survival

P-gp, P-glycoprotein (Abcb1, Mdr1)

RED, rapid equilibrium dialysis

TKO, triple-knockout (*Mdr1a/b*$^{-/-}$ *Bcrp1*$^{-/-}$, P-gp and Bcrp deficient)

Tmax, time at the maximum drug concentration

Vd, volume of distribution

WT, wild-type

Recommended section

Metabolism, Transport, and Pharmacogenomics

JPET Fast Forward. Published on January 8, 2019 as DOI: 10.1124/jpet.118.253708
This article has not been copyedited and formatted. The final version may differ from this version.

Abstract

Targeted inhibition of RAF and MEK by molecularly-targeted agents has been employed as a strategy to block aberrant MAPK signaling in melanoma. While the use of BRAF and MEK inhibitors, either as a single agent or in combination, improved efficacy in BRAF-mutant melanoma, initial responses are often followed by relapse due to acquired resistance. Moreover, some BRAF inhibitors are associated with a paradoxical activation of the MAPK pathway, causing the development of secondary malignancies. The use of panRAF inhibitors, i.e., those that target all isoforms of RAF, may overcome paradoxical activation and resistance. The purpose of this study was to perform a quantitative assessment and evaluation of the influence of efflux mechanisms at the BBB in particular, Abcb1/P-gp and Abcg2/Bcrp, on the brain distribution of three panRAF inhibitors: CCT196969, LY3009120 and MLN2480. In vitro studies using transfected MDCKII cells indicate that only LY3009120 and MLN2480 are substrates of Bcrp, and none of the three inhibitors are substrates of P-gp. The three panRAF inhibitors show high non-specific binding in brain and plasma. In vivo studies in mice show that the brain distribution of CCT196969, LY3009120 and MLN2480 is limited, and is enhanced in transgenic mice lacking P-gp and Bcrp. While MLN2480 has a higher brain distribution, LY3009120 exhibits superior in vitro efficacy in patient-derived melanoma cell lines. The delivery of a drug to the site of action residing behind a functionally intact BBB along with drug potency against the target, collectively play a critical role in determining in vivo efficacy outcomes.

JPET Fast Forward. Published on January 8, 2019 as DOI: 10.1124/jpet.118.253708
This article has not been copyedited and formatted. The final version may differ from this version.

Introduction

Deregulated signaling of the mitogen-activated protein kinase (MAPK) pathway is commonly associated with melanomas, and often occurs due to activating mutations in BRAF (~50%) and NRAS (~20%) (Davies et al., 2002, Hocker and Tsao, 2007, Hodis et al., 2012). Inhibition of MAPK signaling by targeting RAF and MEK has been recognized as an important treatment strategy in BRAF-mutant melanomas (Samatar and Poulikakos, 2014). The improved clinical outcomes with BRAF and MEK inhibitors, either as single agents or in combination, has led to the FDA approval of BRAF inhibitors, vemurafenib, dabrafenib, encorafenib, and MEK inhibitors, cobimetinib, trametinib, binimetinib (Chapman et al., 2011, Flaherty; Infante; et al., 2012, Flaherty; Robert; et al., 2012, Long et al., 2014, Larkin et al., 2014, Ascierto et al., 2013, Delord et al., 2017, Dummer et al., 2018, Dummer et al., 2017).

A persistent clinical challenge in the management of BRAF-mutant melanomas is resistance to BRAF inhibitor therapy, both intrinsic and acquired (Shi et al., 2014, Samatar and Poulikakos, 2014). One approach to overcome resistance is combination therapy with BRAF and MEK inhibitors, causing a vertical blockade of the MAPK pathway at two central nodes. Though such combinations have improved clinical responses, patients still progress due to therapeutic resistance (Wagle et al., 2014, Welsh et al., 2016). Multiple mechanisms of acquired resistance have been identified, and reactivation of the MAPK pathway by acquisition of secondary mutations, such as mutations in RAS, is a common resistance mechanism (Shi et al., 2014, Welsh et al., 2016, Johnson et al., 2015).

In addition, BRAF inhibitors have been attributed to cause a paradoxical activation of the MAPK signaling in RAS-mutant melanomas, triggering the development of secondary malignancies (Hatzivassiliou et al., 2010, Heidorn et al., 2010, Poulikakos et al., 2010). By occupying one partner in homo- and hetero-dimers of RAF, particularly in wild-type BRAF and RAS-mutant melanomas, many BRAF inhibitors promote transactivation of the drug free partner leading to a paradoxical activation of the MAPK pathway (Poulikakos et al., 2010, Samatar and Poulikakos, 2014). Consequently, BRAF inhibitors are contraindicated in wild-type BRAF melanomas (Hatzivassiliou et al., 2010). Inhibitors targeting all isoforms of RAF, i.e., panRAF inhibitors, may show benefits by occupying and inhibiting both partners in RAF dimers, and causing a more effective blockade of the MAPK signaling. Given this multiple isoform blockade, panRAF inhibitors may be useful for first-line treatment of BRAF- and NRAS-mutant melanomas, and also as second-line treatment options in drug-resistant melanomas (Girotti et al., 2015). Furthermore, panRAF/MEK inhibitor combination may be a rational treatment strategy, especially in patients with acquired or intrinsic resistance to MAPK inhibitors (Atefi et al., 2015, Whittaker et al., 2015).

JPET Fast Forward. Published on January 8, 2019 as DOI: 10.1124/jpet.118.253708
This article has not been copyedited and formatted. The final version may differ from this version.

Another challenge is the effective management of melanoma patients with brain metastases. Approximately 70% of patients with metastatic melanoma will develop brain metastases, and after diagnosis of brain metastases, the median overall survival (OS) is less than 8 months (Gupta et al., 1997, Barnholtz-Sloan et al., 2004, Spagnolo et al., 2016). Several anti-cancer therapies have a restricted ability to penetrate an intact blood-brain barrier (BBB), leading to the establishment of a pharmacological sanctuary for tumor cells, thereby limiting their efficacy in the treatment of tumors in the brain (Gampa et al., 2016, Gampa et al., 2017, Kim et al., 2018). A key mechanism responsible for restricting drug delivery to the brain is active efflux at the BBB, often mediated by p-glycoprotein (Abcb1/P-gp) and breast cancer resistance protein (Abcg2/Bcrp) (Kim et al., 2018, Gampa et al., 2016, Gampa et al., 2017). Previous studies have indicated that vemurafenib, dabrafenib, encorafenib, trametinib, cobimetinib and binimetinib will have limited brain distribution due to efflux by P-gp and/or Bcrp (Mittapalli et al., 2013, Mittapalli et al., 2012, Choo et al., 2014, Vaidhyanathan et al., 2014, Wang et al., 2018, de Gooijer et al., 2018). The drug delivery to brain tumors with heterogeneous disruption of the BBB can be highly variable for compounds that show a limited BBB penetration. While the BBB in the core of larger tumors may be relatively compromised, there can be regions within larger tumors, micrometastases and infiltrative tumor sites with a functionally intact BBB and thus have restricted drug distribution (Lockman et al., 2010, Osswald et al., 2016). Given this, development of potent targeted therapies capable of permeating an intact BBB is critical to improve clinical outcomes in patients with melanoma brain metastases (MBM).

CCT196969, LY3009120 and MLN2480 (Fig. 1, Table 1) are panRAF inhibitors that inhibit MAPK signaling with minimal paradoxical activation (Girotti et al., 2015, Henry et al., 2015, Rasco et al., 2013). CCT196969 has low nanomolar IC_{50} against BRAF and CRAF, and also is a potent inhibitor of SRC (Fig. 2). CCT196969 shows efficacy in melanoma cells and patient-derived xenografts that are resistant to BRAF inhibitors and BRAF/MEK inhibitor combinations (Girotti et al., 2015). LY3009120 exhibits low nanomolar potency against ARAF, BRAF and CRAF, and shows activity in preclinical melanoma models (Fig. 2) (Henry et al., 2015, Peng et al., 2015, Chen et al., 2016). MLN2480 has a low nanomolar IC_{50} against BRAF and CRAF, and shows activity in BRAF-mutant tumors, including melanoma, in preclinical models (Sun et al., 2017, Elenbaas B, 2010). LY3009120 and MLN2480 are currently in phase I/II clinical testing (clinicaltrials.gov).

The objective of this study is to evaluate the brain distribution of CCT196969, LY3009120 and MLN2480, and examine the role of P-gp and/or Bcrp in limiting their brain delivery. Anti-RAF therapy is routinely used in

combination with MEK inhibitors for the management of melanoma patients. The newer panRAF inhibitors have advantages over the traditional BRAF inhibitors, and as such panRAF/MEK inhibitor combinations may result in potential benefits in melanoma patients. However, to be effective in brain metastases, drug delivery to target sites in the brain is a key consideration. Given this, evaluation of the distribution of panRAF inhibitors to the brain is important to understand their utility in the treatment of MBM.

Materials and methods

Chemicals

CCT196969, 1-(3-(tert-butyl)-1-phenyl-1H-pyrazol-5-yl)-3-(2-fluoro-4-((3-oxo-3,4-dihydropyrido[2,3-b]pyrazin-8-yl)oxy)phenyl)urea, vemurafenib and dabrafenib were purchased from ChemieTek (Indianapolis, IN). LY3009120, 1-(3,3-Dimethylbutyl)-3-(2-fluoro-4-methyl-5-(7-methyl-2-(methylamino)pyrido(2,3-d)pyrimidin-6-yl)phenyl)urea, was purchased from Selleck Chemicals (Houston, TX). MLN2480, 4-Pyrimidinecarboxamide, 6-amino-5-chloro-N-[(1R)-1-[5-[[[5-chloro-4-(trifluoromethyl)-2-pyridinyl]amino]carbonyl]-2-thiazolyl]ethyl]-, was purchased from Medchem Express (Monmouth Junction, NJ). [^{3}H]-Vinblastine was purchased from Moravek Biochemicals (La Brea, CA). [^{3}H]-Prazosin was purchased from PerkinElmer Life and Analytical Sciences (Waltham, MA). Ko143 [(3S,6S,12aS)-1,2,3,4,6,7,12,12a-octahydro-9-methoxy-6-(2-methylpropyl)-1,4-dioxopyrazino(1',2':1,6) pyrido(3,4-b)indole-3-propanoic acid 1,1-dimethylethyl ester] was purchased from Tocris Bioscience (Ellisville, MO). Zosuquidar [LY335979, (R)-4-([1aR, 6R,10bS]-1,2-difluoro-1,1a,6,10b-tetrahydrodibenzo-[a,e] cyclopropa [c]cycloheptan-6-yl)-([5-quinoloyloxy] methyl)-1-piperazine ethanol, trihydrochloride] was provided by Eli Lilly and Co. (Indianapolis, IN). Cell culture reagents were purchased from Invitrogen (Carlsbad, CA), and all other chemicals used were of high-performance-liquid-chromatography or reagent grade and were obtained from Sigma-Aldrich (St. Louis, MO).

In vitro accumulation studies

Polarized Madin-Darby canine kidney II (MDCKII) cells were used for in vitro cell accumulation studies. MDCKII-wild-type (vector control) and Bcrp1-transfected (MDCKII-Bcrp1) cell lines were a kind gift from Dr. Alfred Schinkel (The Netherlands Cancer Institute). MDCKII-wild type (vector control) and human P-glycoprotein (MDR1)-transfected (MDCKII-MDR1) cell lines were kindly provided by Dr. Piet Borst (The Netherlands Cancer Institute). Cells were cultured in Dulbecco's modified Eagle's medium supplemented with 10% (v/v) fetal bovine serum, and antibiotics (penicillin, 100 U/ml and streptomycin, 100 μg/ml). Cells were grown in 25 mL tissue culture-treated flasks before seeding for the intracellular accumulation experiments, and were maintained at 37°C in a humidified incubator with 5% carbon dioxide.

The intracellular accumulation assays were performed in 12-well polystyrene plates (Corning Glassworks, Corning, NY). In brief, cells were seeded at a density of 2 x 10^5 cells and grown until ~80% confluent. On the day of

experiment, culture media was aspirated and cells were washed two times with warm cell assay buffer (122 mM NaCl, 25 mM $NaHCO_3$, 10 mM glucose, 10 mM HEPES, 3 mM KCl, 2.5 mM $MgSO_4$, 1.8 mM $CaCl_2$, and 0.4 mM K_2HPO_4). The cells were then pre-incubated with cell assay buffer for 30 min, after which the buffer was aspirated and the experiment was initiated by adding 1 mL assay buffer containing 2 μM drug into each well, with further incubation for 60 minutes in an orbital shaker (ShelLab, Cornelius, OR) maintained at 37°C and 60 rpm. The drug solution was aspirated after a 60-minute incubation, followed by washing twice with ice-cold phosphate-buffered saline (PBS), and addition of 500 μL of 1% Triton-X100 to each well for cell lysis. When an inhibitor was used, it was included in both pre-incubation and accumulation steps. The concentration of the drug of interest in solubilized cell fractions was analyzed using liquid chromatography–tandem mass spectrometry (LC-MS/ MS) as described below, and was normalized to protein content that was analyzed using a BCA protein assay (Thermo Scientific Pierce).

In vitro binding assays for determination of unbound (free) fractions

The unbound fractions of the panRAF inhibitors in plasma, brain and serum-containing cell culture media (10% fetal bovine serum, v/v) were determined by performing rapid equilibrium dialysis (RED) experiments as per the protocol described by the manufacturer, with some modifications suggested in the literature (Kalvass and Maurer, 2002, Friden et al., 2007). Preliminary experiments conducted at two concentrations (5 μM and 10 μM) and two time points (4 hr and 6 hr) suggest that the unbound fractions were linear across these concentrations and equilibrium was achieved by 4 hr, for each of the three inhibitors. Consequently, unbound fractions determined at 5 μM concentrations and 4 hr time point were utilized for estimation of Kp,uu and free concentrations. A RED base plate (Thermo Fisher Scientific), and single use RED inserts (Thermo Fisher Scientific) with 8 kDa molecular weight cut off (MWCO) were used for these experiments. Briefly, fresh plasma and brain homogenates (prepared in 3 volumes of PBS, w/v) isolated from wild-type FVB mice, and cell culture media were used. The drug stock in DMSO (1 mg/mL) was spiked in each matrix to obtain final concentrations of 5 μM. 300 μL of 5 μM drug spiked matrix was placed in sample chamber (donor), and 500 μL of phosphate buffered saline (1x PBS at pH 7.4; 100 mM sodium phosphate and 150 mM sodium chloride) was placed in buffer chamber (receiver) of the RED inserts in triplicates. The inserts were placed in a base plate, the assembly covered with sealing tape and incubated on an orbital shaker (ShelLab, Cornelius, OR) at 37°C and 300 rpm for 4 hours. The samples collected after dialysis were stored at -80°C until subsequent LC-MS/MS analysis.

JPET Fast Forward. Published on January 8, 2019 as DOI: 10.1124/jpet.118.253708
This article has not been copyedited and formatted. The final version may differ from this version.

In vitro cytotoxicity assays in patient-derived melanoma cell lines

Short-term cultured human primary melanoma cells (BRAF-mutant M12 or BRAF-mutant M27 or NRAS-mutant M15) were maintained through serial passages in mice via subcutaneous flank implantation in immune-deficient mice (Carlson et al., 2011). Dulbecco's modified Eagle's medium supplemented with 10% (v/v) fetal bovine serum and antibiotics (penicillin, 100 U/ml and streptomycin, 100 μg/ml) was used for growing the explant cultures that were maintained at 37°C in a humidified incubator with 5% carbon dioxide.

For the determination of in vitro drug potency, melanoma cells (M12 or M27 or M15) were seeded into 96-well black clear bottom plates (Corning Incorporated, Corning, NY) at a density of 3500 cells per well in 100 μL of culture media. At 24 hours following plating (~80% confluency), the cells were treated with 9 concentrations of drug in media (n = 6 per concentration). The plates were incubated for 5 days after treatment. The cell viability in each well was determined using a CyQuant cell proliferation assay (Invitrogen) and fluorescence measurement using a BioTek Synergy HT plate reader. The relative survival of cells in the presence of drugs was normalized to the untreated controls.

In vivo studies

Animals: Friend leukemia virus strain B (FVB) wild-type (WT) and triple knockout (*Mdr1a/b*$^{-/-}$ *Bcrp1*$^{-/-}$, TKO, P-gp and Bcrp deficient) mice, balanced for sex, were used in the in vivo studies (Taconic Farms, Germantown, NY). All mice used were 8-16 week-old adults, approximately 15 - 35 g at the time of experiments. Mice were maintained in a 12-hour light/dark cycle with unlimited access to food and water. All studies carried out were in agreement with the guidelines set by Principles of Laboratory Animal Care (National Institutes of Health, Bethesda, MD), and approved by Institutional Animal Care and Use Committee (IACUC) at University of Minnesota.

Plasma and brain pharmacokinetics following intravenous and oral administration of panRAF inhibitors: All dosing solutions were prepared on the day of the experiment. A single intravenous dose of 5 mg/kg CCT196969 (vehicle: dimethyl sulfoxide, Tween 80 and distilled water in a volume ratio of 10:2.5:87.5) was administered to FVB wild-type mice. Blood and brain samples were harvested at 0.17, 0.5, 1, 2, 4, 8 and 14 hours post-dose (n = 4 at each time point). In another oral dosing study, FVB wild-type mice received a single dose of 10 mg/kg CCT196969 via oral gavage (vehicle: 5% dimethyl sulfoxide; percentage grams per volume). Brain and blood samples were collected at 0.17, 0.5, 1, 2, 4, 6, 8, 11 and 14 hours post dose (n = 4 per time point).

Brain distribution studies following single intravenous and oral doses of LY3009120 were also conducted. A single intravenous dose of 5 mg/kg LY3009120 (vehicle: dimethyl sulfoxide, propylene glycol, Cremophor EL and distilled water in a volume ratio of 30:20:10:40) was administered to FVB wild-type mice. Blood and brain samples were harvested at 0.17, 0.5, 1, 2, 4, 7 and 11 hours post-dose (n = 4 at each time point). In the oral dosing study, FVB wild-type mice received a single dose of 25 mg/kg LY3009120 via oral gavage (vehicle: 20% hydroxyl propyl β cyclodextrin; percentage grams per volume). Brain and blood samples were collected at 0.17, 0.5, 1, 2, 4, 8 and 15 hours post dose (n = 4 per time point).

The brain distribution of MLN2480 was determined following administration of a single intravenous dose of 5 mg/kg MLN2480 (vehicle: dimethyl sulfoxide, tween 80 and distilled water in a volume ratio of 10:2.5:87.5) to FVB wild-type mice. Blood and brain samples were harvested at 0.17, 0.5, 1, 2, 4, 8 and 14 hours post-dose (n = 4 at each time point).

In another vivo brain distribution study, FVB wild-type and *Mdr1a/b*$^{-/-}$ *Bcrp1*$^{-/-}$ mice were administered a single oral dose of CCT196969 (5 mg/kg) or LY3009120 (10 mg/kg) or MLN2480 (10 mg/kg). Blood and brain samples were harvested 1-hour post-dose (n = 4).

A serial sacrifice (destructive sampling) design was employed for sampling in the pharmacokinetic studies. At the desired sampling time point, mice were euthanized using a carbon dioxide chamber. Blood was collected by cardiac puncture and transferred to heparinized tubes. The whole brain was removed from the skull and rinsed with ice-cold distilled water, and superficial meninges were removed by blotting with tissue paper. Plasma was separated by centrifugation of whole blood samples at 3500 rpm and 4°C for 15 minutes. Both plasma and brain samples were stored at -80°C, until analysis for drug concentrations by LC-MS/MS. The concentrations in brain were corrected for residual drug in brain vasculature, assuming a vascular volume of 1.4% in mouse brain (Dai et al., 2003).

Steady-state brain distribution of panRAF inhibitors

The determination of steady-state plasma and brain concentrations of panRAF inhibitors was accomplished by implanting Alzet osmotic mini pumps (model 1003D; Durect Corporation, Cupertino, CA) loaded with CCT196969 (5 mg/mL in dimethyl sulfoxide) or LY3009120 (3 mg/mL in dimethyl sulfoxide) or MLN2480 (5 mg/mL in dimethyl sulfoxide) in the peritoneal cavity of wild-type and *Mdr1a/b*$^{-/-}$ *Bcrp1*$^{-/-}$ mice to deliver 1 μL/h drug solution as a constant infusion. The minipumps were loaded with drug solution on the day before the experiment and primed

overnight in sterile PBS at 37°C. The pumps were implanted into the peritoneal cavity as described previously (Agarwal et al., 2013). Briefly, mice were anaesthetized using isoflurane, and the hair on the abdominal cavity was removed. A small incision was made in the skin on the lower right abdomen, followed by an incision in the exposed peritoneal membrane under the cutaneous opening, and the primed pump was inserted into the peritoneal cavity. The peritoneal membrane was sutured with absorbable sutures, and the opening in the skin was sealed with surgical clips. The whole procedure was performed on a heating pad until the animals fully recovered from the anesthesia. Forty-eight hours following pump implantation, the mice were sacrificed, and blood and brain samples were collected. Plasma was obtained by centrifugation of whole blood samples at 3500 rpm and 4°C for 15 minutes. Samples were stored at -80°C until analysis by LC-MS/MS.

LC-MS/MS analysis

The concentrations of drugs in all samples from in vitro and in vivo studies were determined using specific and sensitive LC-MS/MS assays. Brain samples were homogenized using a mechanical homogenizer (PowerGen 125; Thermo Fisher Scientific, Waltham, MA) following the addition of three volumes of 5% bovine serum albumin (BSA) to obtain uniform homogenates. For analysis of unknowns, an aliquot of sample was spiked with 250 ng of MLN2480 or 50 ng of dabrafenib or 10 ng of CCT196969 as internal standards for analysis of CCT196969, LY3009120 and MLN2480, respectively. Liquid-liquid extraction was performed by addition of 5-10 volumes of ethyl acetate, followed by vigorous shaking for 5 minutes and centrifugation at 7500 rpm and 4°C for 5 minutes. The organic layer was separated and transferred to microcentrifuge tubes, and dried under nitrogen gas. The dried residue was reconstituted in 100 µL of mobile phase and transferred into high-performance-liquid-chromatography glass vials with disposable microinserts. The chromatographic analysis was performed on an AQUITY UPLC system (Waters, Milford, MA) using a Phenomenex Gemini 3 µ NX-C18 110A^0 column (50 mm length x 4.6 mm ID; Torrance, CA). The mobile phase (0.1% formic acid in water (A) and 0.1% formic acid in methanol (B)) was delivered at a constant flow rate of 0.35 mL/min. An isocratic method (43% A and 57% B) was employed for CCT19696 and MLN2480, and a gradient method was employed for LY3009120 analysis. The gradient for LY3009120 was as follows: started with 50% B at 0 minutes, held at 50% B for 2 minutes, increased to 90% B over 1 minute, maintained at 90% B for 1 minute, decreased to 50% B over 0.25 minutes and maintained at 50% B for the remainder of 7 minutes.

JPET Fast Forward. Published on January 8, 2019 as DOI: 10.1124/jpet.118.253708
This article has not been copyedited and formatted. The final version may differ from this version.

The column effluent was monitored using a Micromass Quattro Ultima mass spectrometer (Waters, Milford, MA). The instrument was equipped with an electrospray interface, and controlled by the MassLynx (Version 4.1; Waters) data system. The samples were analyzed using an electrospray probe in negative-ionization mode operating at a spray voltage of 4.5 kV for CCT196969 and MLN2480, and positive-ionization mode operating at a spray voltage of 5 kV for LY3009120 and dabrafenib. Samples were introduced into the interface through a heated probe, in which the source temperature and desolvation temperature were set at 100°C and 350°C, respectively. The m/z transitions were 511.98 - 270.85, 425.08 - 324.00, 505.90 - 284.23 and 519.88 - 306.91 for CCT196969, LY3009120, MLN2480 and dabrafenib, respectively. The retention times for CCT19696, LY3009120, MLN2480 and dabrafenib were 3.23, 3.59, 3.10 and 4.65 minutes, respectively. The runtime was 5.5 minutes for CCT196969 and MLN2480, and 7 minutes for LY3009120. Three quality controls, representing low, medium and high concentration ranges in the calibration curve, were used to determine the between-run (interday) precision and accuracy for each of the three compounds. Precision has been expressed as percent coefficient of variation (CV%), while accuracy is expressed as percent bias. For the LC-MS/MS assays of CCT196969, LY3009120 and MLN2480, the percent biases were less than 7%, 11% and 6%, and the percent CVs were less than 12%, 15% and 7%, respectively.

Calculations

The unbound (free) fractions (fu) in plasma, brain homogenate, and serum-containing cell culture media were calculated as the ratio of concentrations of the compound under investigation in buffer to matrix (Kalvass and Maurer, 2002).

$$\text{fu, diluted} = \frac{\text{Drug concentration in buffer (receiver)}}{\text{Drug concentration in matrix (donor)}} \quad (Equation\ 1)$$

The unbound fraction in brain was determined from the measured unbound fraction in diluted brain homogenate (fu,diluted), using the following equation (Kalvass and Maurer, 2002).

$$\text{fu, brain} = \frac{1/\text{D}}{(1/\text{fu, diluted} - 1) + 1/\text{D}} \quad (Equation\ 2)$$

where D (equal to 4) represents a dilution factor, accounting for the diluted brain homogenate.

The brain-to-plasma ratio (Kp) was calculated as the ratio of AUC_{brain} to AUC_{plasma}.

$$\text{Kp} = \frac{\text{AUCbrain}}{\text{AUCplasma}} \quad (Equation\ 4)$$

JPET Fast Forward. Published on January 8, 2019 as DOI: 10.1124/jpet.118.253708
This article has not been copyedited and formatted. The final version may differ from this version.

A comparison of relative drug exposure in the brains of wild-type and knockout (*Mdr1a/b*$^{-/-}$ *Bcrp1*$^{-/-}$) mice was made using the distribution advantage (DA), which was calculated as the Kp in the strain under consideration normalized by the Kp in wild-type mice.

$$\mathrm{DA} = \frac{\mathrm{Kp}, knockout}{\mathrm{Kp}, wild\ type} \quad (Equation\ 5)$$

The unbound partition coefficient, referred to as Kp,uu, was determined using the following equation.

$$\mathrm{Kp,uu} = \frac{\mathrm{AUCbrain\ x\ fu,brain}}{\mathrm{AUCplasma\ x\ fu,plasma}} \quad (Equation\ 6)$$

The data from in vitro cytotoxicity experiments was fitted to "log(inhibitor) vs. normalized response - variable slope" equation using GraphPad Prism version 6.04 (GraphPad, La Jolla, CA) software to determine the IC_{50} of the compounds of interest in the cell lines tested.

Pharmacokinetic data analysis

Pharmacokinetic parameters from the concentration-time profiles in plasma and brain were obtained by non-compartmental analysis (NCA) performed using Phoenix WinNonlin version 6.4 (Certara USA, Inc., Princeton, NJ). The areas under the concentration-time curve (AUC) for plasma (AUC_{plasma}) and brain (AUC_{brain}) were calculated using the linear trapezoidal method. The standard errors around the means of AUC and Cmax were estimated using the sparse sampling module in WinNonlin (Nedelman and Jia, 1998).

Statistical analysis

GraphPad Prism version 6.04 (GraphPad, La Jolla, CA) software was used for statistical analysis. The sample sizes used were based on previous work and were determined based on approximately 80% power to detect 50% difference between groups. Data from all experiments are represented as mean ± standard deviation (S.D.) or mean ± standard error of the mean (S.E.M), unless otherwise indicated. Comparisons between two groups were made using an unpaired t-test. Comparisons between multiple groups were made using one-way analysis of variance (ANOVA), followed by Bonferroni's multiple comparison test. A significance level of $P < 0.05$ was used for all statistical analysis.

JPET Fast Forward. Published on January 8, 2019 as DOI: 10.1124/jpet.118.253708
This article has not been copyedited and formatted. The final version may differ from this version.

Results

In vitro accumulation of panRAF inhibitors in MDCKII-Bcrp1 and MDCKII-MDR1 cells

The intracellular accumulation of CCT196969, LY3009120 and MLN2480 in MDCKII wild-type (vector control), Bcrp1-transfected (MDCKII-Bcrp1), and P-gp-transfected (MDCKII-MDR1) cell lines is summarized in Fig. 3. [^{3}H]-Prazosin and [^{3}H]-vinblastine were used as positive controls for Bcrp1 and MDR1 function, respectively. The cellular accumulation of [^{3}H]-prazosin is significantly lower in Bcrp1-transfected cells compared to wild-type controls (WT: 100±8%; Bcrp1: 24±2%; P<0.0001), and such an effect is abolished in the presence 0.2 μM Ko143, a specific Bcrp1 inhibitor. The cellular accumulation of [^{3}H]-vinblastine is also significantly lower in MDR1-transfected cells than in wild-type controls (WT: 100±1%; MDR1: 9±4%; P<0.0001), and such an effect is abolished in the presence of 1 μM LY335979, a specific P-gp inhibitor. The results confirm a significant elevation in functional activity of efflux transporters in the pertinent transfected cell lines.

In the same experiment, incubation with 2 μM solution of each of the three panRAF inhibitors showed that the accumulation is significantly different in Bcrp1 cells when compared with corresponding wild-type controls for LY3009120 (WT: 100±12%; Bcrp1: 30±7%; P<0.001), and MLN2480 (WT: 100±10%; Bcrp1: 49±10%; P<0.01). The addition of 0.2 μM Ko143 to the Bcrp1 cells caused a reversal of Bcrp1 mediated efflux of LY3009120 and MLN2480. For CCT196969, the cellular accumulation is not significantly different in Bcrp1 cells when compared with corresponding wild-type controls (WT: 100±35%; Bcrp1: 60±20%; ns, P=0.16), and the addition of 0.2 μM Ko143 to Bcrp1 cells did not lead to significant differences in intracellular accumulation. Incubation with 2 μM drug solution shows no significant difference in cellular accumulation in MDR1 cells when compared with corresponding wild-type controls for CCT196969 (WT: 100±32%; MDR1: 83±15%; ns, P=0.56), LY3009120 (WT: 100±27%; MDR1: 72±40%; ns, P=0.46), and MLN2480 (WT: 100±3%; MDR1: 48±25%; ns, P=0.07). Also, the addition of 1 μM LY335979 to MDR1 cells did not lead to significant differences in intracellular accumulation when compared to transfected cells without inhibitor. These in vitro results indicate that only LY3009120 and MLN2480 are substrates of Bcrp1, and none of the three panRAF inhibitors are substrates of P-gp.

Unbound (free) fractions of panRAF inhibitors in matrices of interest

In vitro rapid equilibrium dialysis technique was employed for the determination of unbound fraction (fu) (equations 1 and 2) of panRAF inhibitors in plasma, brain and serum-containing cell culture media. The percent unbound

JPET Fast Forward. Published on January 8, 2019 as DOI: 10.1124/jpet.118.253708
This article has not been copyedited and formatted. The final version may differ from this version.

fractions for CCT196969, LY3009120 and MLN2480 in plasma, brain and cell culture media are as reported in Table 2. The three panRAF inhibitors exhibit high binding in plasma and brain. The estimated unbound fractions in plasma and brain were used for the determination of unbound partition coefficient, Kp,uu, and the unbound fraction in cell culture media was utilized in the estimation of free IC_{50} of the three panRAF inhibitors in each of the cell lines tested.

In vitro efficacy in patient-derived melanoma cell lines

The in vitro efficacy studies were performed in BRAF-mutant M12, BRAF-mutant M27, and NRAS-mutant M15 patient-derived melanoma cell lines. The total IC_{50} for vemurafenib (control), CCT196969, LY3009120 and MLN2480 were estimated using the total drug concentration-response curves determined in the three patient-derived melanoma cell lines. The free fractions in cell culture media for CCT196969, LY3009120 and MLN2480 were used together with the total IC_{50} estimates to determine the free IC_{50} values. The dose-response curves for vemurafenib, CCT196969, LY3009120 and MLN2480 in the 3 cells lines tested are shown in Fig. 4, and the IC_{50} values are listed in Table 3., respectively. The results suggest that M12 is the most sensitive line to treatment with the four inhibitors, and LY3009120 exhibits higher potency in each of the three cell lines tested.

Plasma and brain pharmacokinetics in FVB mice

The pharmacokinetic profiles of panRAF inhibitors were determined in FVB wild-type and transporter deficient (knockout) mice following intravenous and oral drug administration. The brain and plasma concentration time profiles and brain-to-plasma ratios in FVB wild-type mice following a single intravenous bolus dose of 5 mg/kg CCT196969, LY3009120 and MLN2480 are as shown in Fig. 5, Fig. 6 and Fig. 7. The total brain concentrations at the indicated time points are significantly lower than the total plasma concentrations for all the three compounds. Table 4 summarizes the estimated pharmacokinetic parameters following intravenous drug administration. The brain-to-plasma AUC ratios (Kp, equation 4) for CCT196969, LY3009120 and MLN2480 are 0.006, 0.05 and 0.20, respectively, and the corresponding Kp,uu (equation 6) are 0.03, 0.02 and 0.05, respectively.

The concentration time profiles and brain-to-plasma ratios in FVB wild-type mice following a single oral dose of 10 mg/kg CCT196969 and 25 mg/kg LY3009120 are shown in Fig. 5 and Fig. 6. The estimated pharmacokinetic parameters are summarized in Table 5. The brain-to-plasma AUC ratios (Kp, equation 4) for CCT196969 and LY3009120 are 0.01 and 0.04, respectively, and are similar to that observed in the intravenous dosing studies. The

JPET Fast Forward. Published on January 8, 2019 as DOI: 10.1124/jpet.118.253708
This article has not been copyedited and formatted. The final version may differ from this version.

corresponding Kp,uu for CCT196969 and LY3009120 (equation 6) are 0.05 and 0.02, respectively. The bioavailability (F) following oral administration is 0.77 for CCT196969 and 0.04 for LY3009120.

The brain and plasma concentrations and brain-to-plasma ratios in FVB wild-type and *Mdr1a/b*$^{-/-}$ *Bcrp1*$^{-/-}$ mice one-hour post oral administration of panRAF inhibitors (5 mg/kg CCT196969, 10 mg/kg LY3009120 and 10 mg/kg MLN2480) are as shown in Fig. 8. The brain concentrations are significantly lower than the plasma concentrations in wild-type mice for all three panRAF inhibitors, and the brain-to-plasma concentration ratios for CCT196969, LY3009120 and MLN2480 are 0.01, 0.05 and 0.24, respectively. The brain-to-plasma concentration ratios in *Mdr1a/b*$^{-/-}$ *Bcrp1*$^{-/-}$ mice are significantly higher than in wild-type mice for CCT196969, LY3009120 and MLN2480, and are 0.02, 0.32 and 2.66, respectively.

Steady-state brain distribution of panRAF inhibitors

The steady-state brain-to-plasma ratios for CCT196969, LY3009120 and MLN2480 are 0.01 ± 0.002, 0.01 ± 0.01, and 0.34 ± 0.10 in wild-type mice, 0.05 ± 0.02, 0.27 ± 0.12, and 2.88 ± 0.31 in *Mdr1a/b*$^{-/-}$ *Bcrp1*$^{-/-}$ mice, respectively (Fig. 9, Table 6). The brain-to-plasma ratios are about 5, 27 and 9-fold higher for CCT196969, LY3009120 and MLN2480 in *Mdr1a/b*$^{-/-}$ *Bcrp1*$^{-/-}$ mice when compared to wild-type mice. These results are similar to the observations from the brain distribution studies in FVB wild-type and *Mdr1a/b*$^{-/-}$ *Bcrp1*$^{-/-}$ mice that evaluated the brain-to-plasma ratios one-hour post oral drug administration. Collectively, the in vivo studies show that the delivery of the three panRAF inhibitors to the brain is restricted, and active efflux by P-gp and/or Bcrp plays a role in limiting their brain distribution.

JPET Fast Forward. Published on January 8, 2019 as DOI: 10.1124/jpet.118.253708
This article has not been copyedited and formatted. The final version may differ from this version.

Discussion

The small molecule molecularly-targeted therapies and immunotherapies approved for the treatment of melanoma have shown improvements in survival by a few months in patients with MBM (Long et al., 2012, Dummer et al., 2014, Spagnolo et al., 2016, Margolin et al., 2012, Goldberg et al., 2016, Ahmed et al., 2016, Tawbi et al., 2018). While such improvements in survival bring new optimism, the management of metastatic disease that has spread to the brain is still challenging (Gampa et al., 2017). The modest efficacy in patients with MBM may be related to factors that include inadequate drug delivery to tumor cells in the brain and specific brain microenvironment driven alterations in gene expression. As a consequence, both drug delivery and resistance concerns should be addressed to improve treatment outcomes in patients with MBM. A novel class of compounds, the panRAF inhibitors, may address both of these issues.

The panRAF inhibitors may show benefits over mutant-BRAF inhibitors in the treatment of melanoma either as single agents or in combination with a MEK inhibitor, due to their ability to overcome paradoxical activation of the MAPK pathway (Girotti et al., 2015, Peng et al., 2015). Several anti-cancer drugs have restricted brain delivery due to active efflux at the BBB, mainly by P-gp and Bcrp (Gampa et al., 2017, Kim et al., 2018). The transport of substrate compounds back into systemic circulation by efflux transporters can prevent drugs with a potential to be efficacious from reaching the target tumor cells residing behind an intact BBB. Given this, an evaluation of the brain distribution and efflux liability of therapies intended for use in CNS disorders is important. Herein we report the findings of the brain distribution, binding and in vitro efficacy studies for three panRAF inhibitors i.e., CCT196969, LY3009120 and MLN2480. The results provide important information on the ability of these compounds to distribute across the BBB, and also allow a correlation of the in vivo concentrations with in vitro efficacy in patient-derived melanoma cell lines that will help inform in vivo efficacy studies.

In vitro intracellular accumulation studies in transfected MDCKII cells overexpressing either murine Bcrp or human P-gp, both important BBB efflux transporters, suggest that only LY3009120 and MLN2480 are substrates of Bcrp, however, none of the three inhibitors were substrates of P-gp (Fig. 3). In vitro rapid equilibrium dialysis experiments indicate that the three panRAF inhibitors exhibit high non-specific binding in brain and plasma (Table 2). The results of the in vitro efficacy testing reveal that M12, a BRAF-mutant melanoma brain metastasis patient-derived model, is the most sensitive line to treatment with CCT196969, LY3009120, MLN2480 and vemurafenib (Fig. 4, Table 3). LY3009120 has a low nanomolar $IC_{50,}$ and is the most potent inhibitor in each of the three cell lines tested.

Subsequently, experiments were conducted in mice to test the influence of P-gp and/or Bcrp on brain distribution of CCT196969, LY3009120 and MLN2480 in vivo. Pharmacokinetic studies in mice following a single intravenous or oral dose indicate that CCT196969, LY3009120 and MLN2480 all have restricted brain delivery (Fig. 5, Fig. 6 and Fig. 7). The bioavailability following oral administration of CCT196969 was promising (~77%) using the current formulation. On the other hand, the oral bioavailability of LY3009120 was poor (<5%) (Table 5). Reports indicate that formulating LY3009120 as an amorphous solid dispersion improves the bioavailability by overcoming solubility limitations (Henry et al., 2015, Peng et al., 2015). The results of steady-state studies show that the brain distribution of CCT196969, LY3009120 and MLN2480 is enhanced in mice lacking P-gp and Bcrp (Fig. 9, Table 6). Also, studies evaluating the brain distribution one-hour post oral administration of the three panRAF inhibitors in wild-type and triple knockout mice (*Mdr1a/b*$^{-/-}$ *Bcrp1*$^{-/-}$) show similar results (Fig. 8). Together, the in vivo brain distribution studies in wild-type and transgenic knockout mice suggest that the delivery of CCT196969, LY3009120 and MLN2480 to brain is limited due to active efflux by P-gp and/or Bcrp at the BBB, with MLN2480 showing greater brain distribution. Furthermore, MLN2480 exhibits higher brain distribution than vemurafenib and dabrafenib (Table 7). However, MLN2480 shows a relatively modest in vitro efficacy, and LY3009120 exhibits superior in vitro efficacy when compared to CCT196969 and MLN2480 in patient-derived melanoma cell lines. These studies highlight the fact that the combination of drug delivery to target site in the brain and drug potency against the target will eventually influence the in vivo efficacy outcomes.

Given the importance of both drug delivery as well as drug potency in dictating treatment outcomes, a correlation of the observed in vivo concentrations of panRAF inhibitors with in vitro potencies is valuable. The average total drug concentrations post intravenous dosing at the measured time points were used together with the unbound fractions in brain and plasma to obtain unbound concentration-time profiles for CCT196969, LY3009120 and MLN2480 in wild-type mice. The unbound concentration-time profiles were then compared to in vitro potency estimates (free IC_{50}) in M12, to evaluate the potential of CCT196969, LY3009120 and MLN2480 in the treatment of MBM (Fig. 10). The selection of cell line was guided by the results of in vitro efficacy experiments, which indicate M12 to be the most sensitive line to treatment with CCT196969, LY3009120 and MLN2480 (Fig. 4, Table 3). The unbound concentration-time profiles in brain and plasma for MLN2480 show that the unbound concentrations are substantially below the free IC_{50} in M12, when administered at a dose of 5 mg/kg intravenously. Assuming that the administration of MLN2480 at the maximum reported dose of 30 mg/kg po in mice (Sun et al., 2017) will result in a

6-fold increase in concentrations (this assumes linear kinetics and oral bioavailability of 100%), the resulting unbound plasma concentrations will just reach the free IC_{50}, and the brain concentrations will still be substantially below the free IC_{50} in M12. For CCT196969, the unbound concentrations in brain are lower and that in plasma are higher (for about 1 hour) than the free IC_{50} following 5 mg/kg iv dose. Considering that the maximum reported dose in mice for CCT196969 is 25 mg/kg po (Girotti et al., 2015) and the oral bioavailability is 77%, the concentrations will be 4-fold higher (again assuming linear kinetics) following an intravenous dose (20 mg/kg) that will result in similar exposure to 25 mg/kg po dose. The 4-fold increase in concentrations will lead to unbound plasma concentrations higher than the free IC_{50} for about 7 hours; however, the unbound brain concentrations will still be substantially below the free IC_{50}. In case of LY3009120, the unbound concentrations in plasma reach levels higher than the free IC_{50} for approximately 7 hours, and the unbound concentrations in brain are higher than the free IC_{50} in M12 for about 2 hours post-dose after 5 mg/kg iv dosing. An intravenous dose of 10 mg/kg LY3009120 was not tolerable in FVB mice. These findings suggest that CCT196969 and LY3009120 will possibly show superior in vivo efficacy in the treatment of systemic melanoma, as the unbound plasma concentrations reach levels higher than the free IC_{50} estimates in M12 for both the compounds. However, the unbound concentrations in brain achieve levels higher than the free IC_{50} in M12 for LY3009120 alone, suggesting possible efficacy benefits with LY3009120 in the treatment of MBM. Given such insights, testing the efficacy of LY3009120 in preclinical models of MBM will be important to evaluate in vivo efficacy.

The responses to treatment with molecularly-targeted therapies have been sub-optimal and variable in patients with MBM. Such outcomes may be related to inadequate drug delivery to tumor cells in the brain and specific brain microenvironment driven changes in gene expression, both critical challenges that need to be addressed for improving the quality of life of MBM patients. The panRAF inhibitors have advantages over mutant-BRAF inhibitors in overcoming resistance and preventing the paradoxical activation of the MAPK pathway. However, the delivery of panRAF inhibitors to the site of action in the brain and their potency against the target tumor cells are key determinants of in vivo efficacy in the treatment of tumors in the brain. A correlation of unbound plasma and brain drug concentrations with in vitro potency estimates in patient-derived melanoma cell lines for CCT196969, LY3009120 and MLN2480 suggests that LY3009120 is a novel panRAF inhibitor with low nanomolar in vitro potency against mutant-BRAF (M12, M27) and NRAS (M15) patient-derived melanoma cell lines, and has adequate brain delivery to achieve therapeutically active concentrations in the brain. The novel mechanism involving

inhibition of all isoforms of RAF, as well as an appropriate balance of potency and brain delivery make LY3009120 a promising candidate for efficacy testing in preclinical models of MBM. Also, evaluating the use of a rational combination of panRAF/MEK inhibitors for achieving a better vertical blockade of MAPK signaling and in vivo efficacy in the treatment of MBM will be of interest. When using combinations, all inhibitors in a combination regimen must have adequate brain delivery to achieve therapeutic concentrations at the sites of action in the brain to elicit the desired therapeutic response, and minimize the emergence of resistance. Remarkable progress has been made in the treatment of melanoma, however, there still remains a need to develop better therapies for MBM, and drug delivery across a functionally intact BBB is an important challenge that needs to be addressed to fulfill this goal.

Acknowledgements

The authors thank Jim Fisher, Clinical Pharmacology Analytical Laboratory, University of Minnesota, for his support in the development of the LC-MS/MS assays.

Authorship contributions

Participated in research design: Gampa, Kim, Mohammad, Sarkaria, Elmquist.

Conducted experiments: Gampa, Kim, Mohammad, Parrish, Mladek.

Performed data analysis: Gampa, Elmquist.

Wrote or contributed to the writing of the manuscript: Gampa, Parrish, Elmquist, Sarkaria.

References

Agarwal, S., P. Manchanda, M. A. Vogelbaum, J. R. Ohlfest, and W. F. Elmquist (2013) Function of the blood-brain barrier and restriction of drug delivery to invasive glioma cells: findings in an orthotopic rat xenograft model of glioma. *Drug Metab Dispos* 41 (1):33-9. doi: 10.1124/dmd.112.048322.

Ahmed, K. A., D. G. Stallworth, Y. Kim, P. A. Johnstone, L. B. Harrison, J. J. Caudell, H. H. Yu, A. B. Etame, J. S. Weber, and G. T. Gibney (2016) Clinical outcomes of melanoma brain metastases treated with stereotactic radiation and anti-PD-1 therapy. *Ann Oncol* 27 (3):434-41. doi: 10.1093/annonc/mdv622.

Ascierto, P. A., D. Schadendorf, C. Berking, S. S. Agarwala, C. M. van Herpen, P. Queirolo, C. U. Blank, A. Hauschild, J. T. Beck, A. St-Pierre, F. Niazi, S. Wandel, M. Peters, A. Zubel, and R. Dummer (2013) MEK162 for patients with advanced melanoma harbouring NRAS or Val600 BRAF mutations: a non-randomised, open-label phase 2 study. *Lancet Oncol* 14 (3):249-56. doi: 10.1016/S1470-2045(13)70024-X.

Atefi, M., B. Titz, E. Avramis, C. Ng, D. J. Wong, A. Lassen, M. Cerniglia, H. Escuin-Ordinas, D. Foulad, B. Comin-Anduix, T. G. Graeber, and A. Ribas (2015) Combination of pan-RAF and MEK inhibitors in NRAS mutant melanoma. *Mol Cancer* 14:27. doi: 10.1186/s12943-015-0293-5.

Barnholtz-Sloan, J. S., A. E. Sloan, F. G. Davis, F. D. Vigneau, P. Lai, and R. E. Sawaya (2004) Incidence proportions of brain metastases in patients diagnosed (1973 to 2001) in the Metropolitan Detroit Cancer Surveillance System. *J Clin Oncol* 22 (14):2865-72. doi: 10.1200/JCO.2004.12.149.

Carlson, B. L., J. L. Pokorny, M. A. Schroeder, and J. N. Sarkaria (2011) Establishment, maintenance and in vitro and in vivo applications of primary human glioblastoma multiforme (GBM) xenograft models for translational biology studies and drug discovery. *Curr Protoc Pharmacol* Chapter 14:Unit 14 16. doi: 10.1002/0471141755.ph1416s52.

Chapman, P. B., A. Hauschild, C. Robert, J. B. Haanen, P. Ascierto, J. Larkin, R. Dummer, C. Garbe, A. Testori, M. Maio, D. Hogg, P. Lorigan, C. Lebbe, T. Jouary, D. Schadendorf, A. Ribas, S. J. O'Day, J. A. Sosman, J. M. Kirkwood, A. M. Eggermont, B. Dreno, K. Nolop, J. Li, B. Nelson, J. Hou, R. J. Lee, K. T. Flaherty, G. A. McArthur, and Brim- Study Group (2011) Improved survival with vemurafenib in melanoma with BRAF V600E mutation. *N Engl J Med* 364 (26):2507-16. doi: 10.1056/NEJMoa1103782.

Chen, S. H., Y. Zhang, R. D. Van Horn, T. Yin, S. Buchanan, V. Yadav, I. Mochalkin, S. S. Wong, Y. G. Yue, L. Huber, I. Conti, J. R. Henry, J. J. Starling, G. D. Plowman, and S. B. Peng (2016) Oncogenic BRAF Deletions That Function as Homodimers and Are Sensitive to Inhibition by RAF Dimer Inhibitor LY3009120. *Cancer Discov* 6 (3):300-15. doi: 10.1158/2159-8290.CD-15-0896.

Choo, E. F., J. Ly, J. Chan, S. K. Shahidi-Latham, K. Messick, E. Plise, C. M. Quiason, and L. Yang (2014) Role of P-glycoprotein on the brain penetration and brain pharmacodynamic activity of the MEK inhibitor cobimetinib. *Mol Pharm* 11 (11):4199-207. doi: 10.1021/mp500435s.

Dai, H., P. Marbach, M. Lemaire, M. Hayes, and W. F. Elmquist (2003) Distribution of STI-571 to the brain is limited by P-glycoprotein-mediated efflux. *J Pharmacol Exp Ther* 304 (3):1085-92. doi: 10.1124/jpet.102.045260.

Davies, H., G. R. Bignell, C. Cox, P. Stephens, S. Edkins, S. Clegg, J. Teague, H. Woffendin, M. J. Garnett, W. Bottomley, N. Davis, E. Dicks, R. Ewing, Y. Floyd, K. Gray, S. Hall, R. Hawes, J. Hughes, V. Kosmidou, A. Menzies, C. Mould, A. Parker, C. Stevens, S. Watt, S. Hooper, R. Wilson, H. Jayatilake, B. A. Gusterson, C. Cooper, J. Shipley, D. Hargrave, K. Pritchard-Jones, N. Maitland, G. Chenevix-Trench, G. J. Riggins, D. D. Bigner, G. Palmieri, A. Cossu, A. Flanagan, A. Nicholson, J. W. Ho, S. Y. Leung, S. T. Yuen, B. L. Weber, H. F. Seigler, T. L. Darrow, H. Paterson, R. Marais, C. J. Marshall, R. Wooster, M. R. Stratton, and P. A. Futreal (2002) Mutations of the BRAF gene in human cancer. *Nature* 417 (6892):949-54. doi: 10.1038/nature00766.

de Gooijer, M. C., P. Zhang, R. Weijer, L. C. M. Buil, J. H. Beijnen, and O. van Tellingen (2018) The impact of P-glycoprotein and breast cancer resistance protein on the brain pharmacokinetics and pharmacodynamics of a panel of MEK inhibitors. *Int J Cancer* 142 (2):381-391. doi: 10.1002/ijc.31052.

Delord, J. P., C. Robert, M. Nyakas, G. A. McArthur, R. Kudchakar, A. Mahipal, Y. Yamada, R. Sullivan, A. Arance, R. F. Kefford, M. S. Carlino, M. Hidalgo, C. Gomez-Roca, D. Michel, A. Seroutou, V. Aslanis, G. Caponigro, D. D. Stuart, L. Moutouh-de Parseval, T. Demuth, and R. Dummer (2017) Phase I Dose-Escalation and -Expansion Study of the BRAF Inhibitor Encorafenib (LGX818) in Metastatic BRAF-Mutant Melanoma. *Clin Cancer Res* 23 (18):5339-5348. doi: 10.1158/1078-0432.CCR-16-2923.

Dummer, R., P. A. Ascierto, H. J. Gogas, A. Arance, M. Mandala, G. Liszkay, C. Garbe, D. Schadendorf, I. Krajsova, R. Gutzmer, V. Chiarion-Sileni, C. Dutriaux, J. W. B. de Groot, N. Yamazaki, C. Loquai, L. A. Moutouh-de Parseval, M. D. Pickard, V. Sandor, C. Robert, and K. T. Flaherty (2018) Encorafenib plus

binimetinib versus vemurafenib or encorafenib in patients with BRAF-mutant melanoma (COLUMBUS): a multicentre, open-label, randomised phase 3 trial. *Lancet Oncol* 19 (5):603-615. doi: 10.1016/S1470-2045(18)30142-6.

Dummer, R., S. M. Goldinger, C. P. Turtschi, N. B. Eggmann, O. Michielin, L. Mitchell, L. Veronese, P. R. Hilfiker, L. Felderer, and J. D. Rinderknecht (2014) Vemurafenib in patients with BRAF(V600) mutation-positive melanoma with symptomatic brain metastases: final results of an open-label pilot study. *Eur J Cancer* 50 (3):611-21. doi: 10.1016/j.ejca.2013.11.002.

Dummer, R., D. Schadendorf, P. A. Ascierto, A. Arance, C. Dutriaux, A. M. Di Giacomo, P. Rutkowski, M. Del Vecchio, R. Gutzmer, M. Mandala, L. Thomas, L. Demidov, C. Garbe, D. Hogg, G. Liszkay, P. Queirolo, E. Wasserman, J. Ford, M. Weill, L. A. Sirulnik, V. Jehl, V. Bozon, G. V. Long, and K. Flaherty (2017) Binimetinib versus dacarbazine in patients with advanced NRAS-mutant melanoma (NEMO): a multicentre, open-label, randomised, phase 3 trial. *Lancet Oncol* 18 (4):435-445. doi: 10.1016/S1470-2045(17)30180-8.

Elenbaas B, Singh L, Boccia A, Cullen P, Peng H, Rohde E, Raimundo B, Kumaravel G, Joseph I. 2010. "BIIB024, a potent pan-Raf kinase inhibitor fro melanoma and solid tumors." EORTC-NCI-AACR Molecular Targets and Cancer Therapeutics, November 16 -19 2010.

Flaherty, K. T., J. R. Infante, A. Daud, R. Gonzalez, R. F. Kefford, J. Sosman, O. Hamid, L. Schuchter, J. Cebon, N. Ibrahim, R. Kudchadkar, H. A. Burris, 3rd, G. Falchook, A. Algazi, K. Lewis, G. V. Long, I. Puzanov, P. Lebowitz, A. Singh, S. Little, P. Sun, A. Allred, D. Ouellet, K. B. Kim, K. Patel, and J. Weber (2012) Combined BRAF and MEK inhibition in melanoma with BRAF V600 mutations. *N Engl J Med* 367 (18):1694-703. doi: 10.1056/NEJMoa1210093.

Flaherty, K. T., C. Robert, P. Hersey, P. Nathan, C. Garbe, M. Milhem, L. V. Demidov, J. C. Hassel, P. Rutkowski, P. Mohr, R. Dummer, U. Trefzer, J. M. Larkin, J. Utikal, B. Dreno, M. Nyakas, M. R. Middleton, J. C. Becker, M. Casey, L. J. Sherman, F. S. Wu, D. Ouellet, A. M. Martin, K. Patel, D. Schadendorf, and Metric Study Group (2012) Improved survival with MEK inhibition in BRAF-mutated melanoma. *N Engl J Med* 367 (2):107-14. doi: 10.1056/NEJMoa1203421.

Friden, M., A. Gupta, M. Antonsson, U. Bredberg, and M. Hammarlund-Udenaes (2007) In vitro methods for estimating unbound drug concentrations in the brain interstitial and intracellular fluids. *Drug Metab Dispos* 35 (9):1711-9. doi: 10.1124/dmd.107.015222.

Gampa, G., S. Vaidhyanathan, B. W. Resman, K. E. Parrish, S. N. Markovic, J. N. Sarkaria, and W. F. Elmquist (2016) Challenges in the delivery of therapies to melanoma brain metastases. *Curr Pharmacol Rep* 2 (6):309-325. doi: 10.1007/s40495-016-0072-z.

Gampa, G., S. Vaidhyanathan, J. N. Sarkaria, and W. F. Elmquist (2017) Drug delivery to melanoma brain metastases: Can current challenges lead to new opportunities? *Pharmacol Res* 123:10-25. doi: 10.1016/j.phrs.2017.06.008.

Girotti, M. R., F. Lopes, N. Preece, D. Niculescu-Duvaz, A. Zambon, L. Davies, S. Whittaker, G. Saturno, A. Viros, M. Pedersen, B. M. Suijkerbuijk, D. Menard, R. McLeary, L. Johnson, L. Fish, S. Ejiama, B. Sanchez-Laorden, J. Hohloch, N. Carragher, K. Macleod, G. Ashton, A. A. Marusiak, A. Fusi, J. Brognard, M. Frame, P. Lorigan, R. Marais, and C. Springer (2015) Paradox-breaking RAF inhibitors that also target SRC are effective in drug-resistant BRAF mutant melanoma. *Cancer Cell* 27 (1):85-96. doi: 10.1016/j.ccell.2014.11.006.

Goldberg, S. B., S. N. Gettinger, A. Mahajan, A. C. Chiang, R. S. Herbst, M. Sznol, A. J. Tsiouris, J. Cohen, A. Vortmeyer, L. Jilaveanu, J. Yu, U. Hegde, S. Speaker, M. Madura, A. Ralabate, A. Rivera, E. Rowen, H. Gerrish, X. Yao, V. Chiang, and H. M. Kluger (2016) Pembrolizumab for patients with melanoma or non-small-cell lung cancer and untreated brain metastases: early analysis of a non-randomised, open-label, phase 2 trial. *Lancet Oncol* 17 (7):976-983. doi: 10.1016/S1470-2045(16)30053-5.

Gupta, G., A. G. Robertson, and R. M. MacKie (1997) Cerebral metastases of cutaneous melanoma. *Br J Cancer* 76 (2):256-9.

Hatzivassiliou, G., K. Song, I. Yen, B. J. Brandhuber, D. J. Anderson, R. Alvarado, M. J. Ludlam, D. Stokoe, S. L. Gloor, G. Vigers, T. Morales, I. Aliagas, B. Liu, S. Sideris, K. P. Hoeflich, B. S. Jaiswal, S. Seshagiri, H. Koeppen, M. Belvin, L. S. Friedman, and S. Malek (2010) RAF inhibitors prime wild-type RAF to activate the MAPK pathway and enhance growth. *Nature* 464 (7287):431-5. doi: 10.1038/nature08833.

Heidorn, S. J., C. Milagre, S. Whittaker, A. Nourry, I. Niculescu-Duvas, N. Dhomen, J. Hussain, J. S. Reis-Filho, C. J. Springer, C. Pritchard, and R. Marais (2010) Kinase-dead BRAF and oncogenic RAS cooperate to drive tumor progression through CRAF. *Cell* 140 (2):209-21. doi: 10.1016/j.cell.2009.12.040.

Henry, J. R., M. D. Kaufman, S. B. Peng, Y. M. Ahn, T. M. Caldwell, L. Vogeti, H. Telikepalli, W. P. Lu, M. M. Hood, T. J. Rutkoski, B. D. Smith, S. Vogeti, D. Miller, S. C. Wise, L. Chun, X. Zhang, Y. Zhang, L. Kays, P. A. Hipskind, A. D. Wrobleski, K. L. Lobb, J. M. Clay, J. D. Cohen, J. L. Walgren, D. McCann, P. Patel, D. K. Clawson, S. Guo, D. Manglicmot, C. Groshong, C. Logan, J. J. Starling, and D. L. Flynn (2015) Discovery of 1-(3,3-dimethylbutyl)-3-(2-fluoro-4-methyl-5-(7-methyl-2-(methylamino)pyrido[2,3-d]pyrimidin-6-yl)phenyl)urea (LY3009120) as a pan-RAF inhibitor with minimal paradoxical activation and activity against BRAF or RAS mutant tumor cells. *J Med Chem* 58 (10):4165-79. doi: 10.1021/acs.jmedchem.5b00067.

Hocker, T., and H. Tsao (2007) Ultraviolet radiation and melanoma: a systematic review and analysis of reported sequence variants. *Hum Mutat* 28 (6):578-88. doi: 10.1002/humu.20481.

Hodis, E., I. R. Watson, G. V. Kryukov, S. T. Arold, M. Imielinski, J. P. Theurillat, E. Nickerson, D. Auclair, L. Li, C. Place, D. Dicara, A. H. Ramos, M. S. Lawrence, K. Cibulskis, A. Sivachenko, D. Voet, G. Saksena, N. Stransky, R. C. Onofrio, W. Winckler, K. Ardlie, N. Wagle, J. Wargo, K. Chong, D. L. Morton, K. Stemke-Hale, G. Chen, M. Noble, M. Meyerson, J. E. Ladbury, M. A. Davies, J. E. Gershenwald, S. N. Wagner, D. S. Hoon, D. Schadendorf, E. S. Lander, S. B. Gabriel, G. Getz, L. A. Garraway, and L. Chin (2012) A landscape of driver mutations in melanoma. *Cell* 150 (2):251-63. doi: 10.1016/j.cell.2012.06.024.

Johnson, D. B., A. M. Menzies, L. Zimmer, Z. Eroglu, F. Ye, S. Zhao, H. Rizos, A. Sucker, R. A. Scolyer, R. Gutzmer, H. Gogas, R. F. Kefford, J. F. Thompson, J. C. Becker, C. Berking, F. Egberts, C. Loquai, S. M. Goldinger, G. M. Pupo, W. Hugo, X. Kong, L. A. Garraway, J. A. Sosman, A. Ribas, R. S. Lo, G. V. Long, and D. Schadendorf (2015) Acquired BRAF inhibitor resistance: A multicenter meta-analysis of the spectrum and frequencies, clinical behaviour, and phenotypic associations of resistance mechanisms. *Eur J Cancer* 51 (18):2792-9. doi: 10.1016/j.ejca.2015.08.022.

Kalvass, J. C., and T. S. Maurer (2002) Influence of nonspecific brain and plasma binding on CNS exposure: implications for rational drug discovery. *Biopharm Drug Dispos* 23 (8):327-38. doi: 10.1002/bdd.325.

Kim, M., S. H. Kizilbash, J. K. Laramy, G. Gampa, K. E. Parrish, J. N. Sarkaria, and W. F. Elmquist (2018) Barriers to Effective Drug Treatment for Brain Metastases: A Multifactorial Problem in the Delivery of Precision Medicine. *Pharm Res* 35 (9):177. doi: 10.1007/s11095-018-2455-9.

Larkin, J., P. A. Ascierto, B. Dreno, V. Atkinson, G. Liszkay, M. Maio, M. Mandala, L. Demidov, D. Stroyakovskiy, L. Thomas, L. de la Cruz-Merino, C. Dutriaux, C. Garbe, M. A. Sovak, I. Chang, N. Choong, S. P. Hack, G. A. McArthur, and A. Ribas (2014) Combined vemurafenib and cobimetinib in BRAF-mutated melanoma. *N Engl J Med* 371 (20):1867-76. doi: 10.1056/NEJMoa1408868.

Lockman, P. R., R. K. Mittapalli, K. S. Taskar, V. Rudraraju, B. Gril, K. A. Bohn, C. E. Adkins, A. Roberts, H. R. Thorsheim, J. A. Gaasch, S. Huang, D. Palmieri, P. S. Steeg, and Q. R. Smith (2010) Heterogeneous blood-tumor barrier permeability determines drug efficacy in experimental brain metastases of breast cancer. *Clin Cancer Res* 16 (23):5664-78. doi: 10.1158/1078-0432.CCR-10-1564.

Long, G. V., D. Stroyakovskiy, H. Gogas, E. Levchenko, F. de Braud, J. Larkin, C. Garbe, T. Jouary, A. Hauschild, J. J. Grob, V. Chiarion Sileni, C. Lebbe, M. Mandala, M. Millward, A. Arance, I. Bondarenko, J. B. Haanen, J. Hansson, J. Utikal, V. Ferraresi, N. Kovalenko, P. Mohr, V. Probachai, D. Schadendorf, P. Nathan, C. Robert, A. Ribas, D. J. DeMarini, J. G. Irani, M. Casey, D. Ouellet, A. M. Martin, N. Le, K. Patel, and K. Flaherty (2014) Combined BRAF and MEK inhibition versus BRAF inhibition alone in melanoma. *N Engl J Med* 371 (20):1877-88. doi: 10.1056/NEJMoa1406037.

Long, G. V., U. Trefzer, M. A. Davies, R. F. Kefford, P. A. Ascierto, P. B. Chapman, I. Puzanov, A. Hauschild, C. Robert, A. Algazi, L. Mortier, H. Tawbi, T. Wilhelm, L. Zimmer, J. Switzky, S. Swann, A. M. Martin, M. Guckert, V. Goodman, M. Streit, J. M. Kirkwood, and D. Schadendorf (2012) Dabrafenib in patients with Val600Glu or Val600Lys BRAF-mutant melanoma metastatic to the brain (BREAK-MB): a multicentre, open-label, phase 2 trial. *Lancet Oncol* 13 (11):1087-95. doi: 10.1016/S1470-2045(12)70431-X.

Margolin, K., M. S. Ernstoff, O. Hamid, D. Lawrence, D. McDermott, I. Puzanov, J. D. Wolchok, J. I. Clark, M. Sznol, T. F. Logan, J. Richards, T. Michener, A. Balogh, K. N. Heller, and F. S. Hodi (2012) Ipilimumab in patients with melanoma and brain metastases: an open-label, phase 2 trial. *Lancet Oncol* 13 (5):459-65. doi: 10.1016/S1470-2045(12)70090-6.

Mittapalli, R. K., S. Vaidhyanathan, A. Z. Dudek, and W. F. Elmquist (2013) Mechanisms limiting distribution of the threonine-protein kinase B-RaF(V600E) inhibitor dabrafenib to the brain: implications for the treatment of melanoma brain metastases. *J Pharmacol Exp Ther* 344 (3):655-64. doi: 10.1124/jpet.112.201475.

Mittapalli, R. K., S. Vaidhyanathan, R. Sane, and W. F. Elmquist (2012) Impact of P-glycoprotein (ABCB1) and breast cancer resistance protein (ABCG2) on the brain distribution of a novel BRAF inhibitor: vemurafenib (PLX4032). *J Pharmacol Exp Ther* 342 (1):33-40. doi: 10.1124/jpet.112.192195.

Nedelman, J. R., and X. Jia (1998) An extension of Satterthwaite's approximation applied to pharmacokinetics. *J Biopharm Stat* 8 (2):317-28. doi: 10.1080/10543409808835241.

Osswald, M., J. Blaes, Y. Liao, G. Solecki, M. Gommel, A. S. Berghoff, L. Salphati, J. J. Wallin, H. S. Phillips, W. Wick, and F. Winkler (2016) Impact of Blood-Brain Barrier Integrity on Tumor Growth and Therapy Response in Brain Metastases. *Clin Cancer Res* 22 (24):6078-6087. doi: 10.1158/1078-0432.CCR-16-1327.

Peng, S. B., J. R. Henry, M. D. Kaufman, W. P. Lu, B. D. Smith, S. Vogeti, T. J. Rutkoski, S. Wise, L. Chun, Y. Zhang, R. D. Van Horn, T. Yin, X. Zhang, V. Yadav, S. H. Chen, X. Gong, X. Ma, Y. Webster, S. Buchanan, I. Mochalkin, L. Huber, L. Kays, G. P. Donoho, J. Walgren, D. McCann, P. Patel, I. Conti, G. D. Plowman, J. J. Starling, and D. L. Flynn (2015) Inhibition of RAF Isoforms and Active Dimers by LY3009120 Leads to Anti-tumor Activities in RAS or BRAF Mutant Cancers. *Cancer Cell* 28 (3):384-98. doi: 10.1016/j.ccell.2015.08.002.

Poulikakos, P. I., C. Zhang, G. Bollag, K. M. Shokat, and N. Rosen (2010) RAF inhibitors transactivate RAF dimers and ERK signalling in cells with wild-type BRAF. *Nature* 464 (7287):427-30. doi: 10.1038/nature08902.

Rasco, D.W. , A. J. Olszanski, A. Patnaik, G. Espino, R. Neuwirth, S. Faucette, M. Bargfrede, E. A. Gangolli, R. M. Walker, M. Kneissl, and V. Bozon (2013) MLN2480, an investigational oral panRAF kinase inhibitor, in patients (pts) with relapsed or refractory solid tumors: Phase I study. *J Clin Oncol* 31.

Samatar, A. A., and P. I. Poulikakos (2014) Targeting RAS-ERK signalling in cancer: promises and challenges. *Nat Rev Drug Discov* 13 (12):928-42. doi: 10.1038/nrd4281.

Shi, H., W. Hugo, X. Kong, A. Hong, R. C. Koya, G. Moriceau, T. Chodon, R. Guo, D. B. Johnson, K. B. Dahlman, M. C. Kelley, R. F. Kefford, B. Chmielowski, J. A. Glaspy, J. A. Sosman, N. van Baren, G. V. Long, A. Ribas, and R. S. Lo (2014) Acquired resistance and clonal evolution in melanoma during BRAF inhibitor therapy. *Cancer Discov* 4 (1):80-93. doi: 10.1158/2159-8290.CD-13-0642.

Spagnolo, F., V. Picasso, M. Lambertini, V. Ottaviano, B. Dozin, and P. Queirolo (2016) Survival of patients with metastatic melanoma and brain metastases in the era of MAP-kinase inhibitors and immunologic checkpoint blockade antibodies: A systematic review. *Cancer Treat Rev* 45:38-45. doi: 10.1016/j.ctrv.2016.03.003.

Sun, Y., J. A. Alberta, C. Pilarz, D. Calligaris, E. J. Chadwick, S. H. Ramkissoon, L. A. Ramkissoon, V. M. Garcia, E. Mazzola, L. Goumnerova, M. Kane, Z. Yao, M. W. Kieran, K. L. Ligon, W. C. Hahn, L. A. Garraway, N. Rosen, N. S. Gray, N. Y. Agar, S. J. Buhrlage, R. A. Segal, and C. D. Stiles (2017) A brain-penetrant RAF dimer antagonist for the noncanonical BRAF oncoprotein of pediatric low-grade astrocytomas. *Neuro Oncol* 19 (6):774-785. doi: 10.1093/neuonc/now261.

Tawbi, H. A., P. A. Forsyth, A. Algazi, O. Hamid, F. S. Hodi, S. J. Moschos, N. I. Khushalani, K. Lewis, C. D. Lao, M. A. Postow, M. B. Atkins, M. S. Ernstoff, D. A. Reardon, I. Puzanov, R. R. Kudchadkar, R. P. Thomas, A. Tarhini, A. C. Pavlick, J. Jiang, A. Avila, S. Demelo, and K. Margolin (2018) Combined Nivolumab and Ipilimumab in Melanoma Metastatic to the Brain. *N Engl J Med* 379 (8):722-730. doi: 10.1056/NEJMoa1805453.

Vaidhyanathan, S., R. K. Mittapalli, J. N. Sarkaria, and W. F. Elmquist (2014) Factors influencing the CNS distribution of a novel MEK-1/2 inhibitor: implications for combination therapy for melanoma brain metastases. *Drug Metab Dispos* 42 (8):1292-300. doi: 10.1124/dmd.114.058339.

Wagle, N., E. M. Van Allen, D. J. Treacy, D. T. Frederick, Z. A. Cooper, A. Taylor-Weiner, M. Rosenberg, E. M. Goetz, R. J. Sullivan, D. N. Farlow, D. C. Friedrich, K. Anderka, D. Perrin, C. M. Johannessen, A. McKenna, K. Cibulskis, G. Kryukov, E. Hodis, D. P. Lawrence, S. Fisher, G. Getz, S. B. Gabriel, S. L. Carter, K. T. Flaherty, J. A. Wargo, and L. A. Garraway (2014) MAP kinase pathway alterations in BRAF-mutant melanoma patients with acquired resistance to combined RAF/MEK inhibition. *Cancer Discov* 4 (1):61-8. doi: 10.1158/2159-8290.CD-13-0631.

Wang, J., C. Gan, R. W. Sparidans, E. Wagenaar, S. van Hoppe, J. H. Beijnen, and A. H. Schinkel (2018) P-glycoprotein (MDR1/ABCB1) and Breast Cancer Resistance Protein (BCRP/ABCG2) affect brain accumulation and intestinal disposition of encorafenib in mice. *Pharmacol Res* 129:414-423. doi: 10.1016/j.phrs.2017.11.006.

Welsh, S. J., H. Rizos, R. A. Scolyer, and G. V. Long (2016) Resistance to combination BRAF and MEK inhibition in metastatic melanoma: Where to next? *Eur J Cancer* 62:76-85. doi: 10.1016/j.ejca.2016.04.005.

Whittaker, S. R., G. S. Cowley, S. Wagner, F. Luo, D. E. Root, and L. A. Garraway (2015) Combined Pan-RAF and MEK Inhibition Overcomes Multiple Resistance Mechanisms to Selective RAF Inhibitors. *Mol Cancer Ther* 14 (12):2700-11. doi: 10.1158/1535-7163.MCT-15-0136-T.

Footnotes

This work was supported by the National Institutes of Health [Grants RO1-NS077921, RO1-NS073610 and U54-CA210180]. Gautham Gampa was supported by the Ronald J. Sawchuk Fellowship in Pharmacokinetics and University of Minnesota Doctoral Dissertation Fellowship (DDF).

JPET Fast Forward. Published on January 8, 2019 as DOI: 10.1124/jpet.118.253708
This article has not been copyedited and formatted. The final version may differ from this version.

Figure legends

Fig 1. Chemical structures of (A) CCT196969, (B) LY3009120, and (C) MLN2480.

Fig 2. Schematic representing the MAPK pathway, and targets of panRAF inhibitors, approved BRAF inhibitors and approved MEK inhibitors.

Fig 3. In vitro intracellular accumulation of panRAF inhibitors. (A) The accumulation of prazosin (Bcrp probe substrate; positive control), CCT196969, LY3009120, and MLN2480 in MDCKII wild-type and Bcrp1-transfected cells with and without Bcrp inhibitor Ko143 (0.2 μM). (B) The accumulation of vinblastine (probe substrate for P-gp/MDR1; positive control), CCT196969, LY3009120, and MLN2480 in wild-type and MDR1-transfected cells with and without P-gp inhibitor LY335979 (1 μM). Data represent the mean ± S.D.; n = 3 for all data points. $$P<$ 0.05 compared with the untreated transfected cell line; ^$P<$ 0.001 compared with the untreated transfected cell line; #$P<$ 0.0001 compared with the untreated transfected cell line; **$P<$ 0.01 compared with respective wild-type controls; ***$P<$ 0.001 compared with respective wild-type controls; ****$P<$ 0.0001 compared with respective wild-type controls.

Fig 4. In vitro efficacy of panRAF inhibitors in patient-derived xenograft melanoma cell lines. (A) Dose-response curves showing the effect of various concentrations of vemurafenib, CCT196969, LY3009120 and MLN2480 on BRAF-mutant M12 melanoma cell line. (B) Growth profiles showing the effect of various concentrations of vemurafenib, CCT196969, LY3009120 and MLN2480 on BRAF-mutant M27 melanoma cell line. (C) Dose-response curves showing the effect of multiple concentrations of vemurafenib, CCT196969, LY3009120 and MLN2480 on NRAS-mutant M15 melanoma cell line. Data represent the mean ± S.E.M.; n = 6 for all data points.

Fig 5. Pharmacokinetic profiles of CCT196969 in FVB wild-type mice following intravenous (i.v.) and oral (p.o.) administration. Plasma and brain concentrations (A), and brain-to-plasma concentration ratios (B) of CCT196969 following administration of single i.v. bolus dose of 5 mg/kg. Plasma and brain concentrations (C), and brain-to-plasma concentration ratios (D) of CCT196969 post single oral dose of 10 mg/kg. Data represent mean ± S.D., n = 4.

Fig 6. Pharmacokinetic profiles of LY3009120 in FVB wild-type mice following intravenous (i.v.) and oral (p.o.) dosing. Plasma and brain concentrations (A), and brain-to-plasma concentration ratios (B) of LY3009120 following administration of single i.v. bolus dose of 5 mg/kg. Plasma and brain concentrations (C), and brain-to-plasma concentration ratios (D) of LY3009120 post single oral dose of 25 mg/kg. Data represent mean ± S.D., n = 4.

Fig 7. Pharmacokinetic profiles of MLN2480 in FVB wild-type mice following intravenous (i.v.) dosing. Plasma and brain concentrations (A), and brain-to-plasma concentration ratios (B) of MLN2480 following administration of single i.v. bolus dose of 5 mg/kg. Data represent mean ± S.D., n = 4.

Fig 8. Brain distribution one-hour following oral administration of panRAF inhibitors in FVB wild-type and *Mdr1a/b*$^{-/-}$ *Bcrp1*$^{-/-}$ mice. *P< 0.05, **P< 0.01 and ****P< 0.0001, for statistical comparison by unpaired t-test. Data represent mean ± S.D., n = 4.

Fig 9. Steady-state brain distribution of panRAF inhibitors in FVB wild-type and *Mdr1a/b*$^{-/-}$ *Bcrp1*$^{-/-}$ mice. (A) Steady-state plasma and brain concentrations of CCT196969, and (B) brain-to-plasma ratios; (C) Steady-state plasma and brain concentrations of LY3009120, and (D) brain-to-plasma ratios; (E) Steady-state plasma and brain concentrations of MLN2480, and (F) brain-to-plasma ratios. **P< 0.01 compared to wild-type brain concentration, ***P< 0.001 compared to wild-type brain concentration, ##P< 0.01 compared to wild-type brain-to-plasma ratio and ###P< 0.001 compared to wild-type brain-to-plasma ratio, for statistical comparison by unpaired t-test. Data represent mean ± S.D., n = 4.

Fig 10. Plasma and brain unbound concentration-time profiles of (A) CCT196969, (B) LY3009120 and (C) MLN2480 in FVB wild-type mice following 5 mg/kg intravenous drug administration. The unbound concentrations were determined using the in vivo concentrations and the unbound fraction (fu) estimates from in vitro rapid equilibrium dialysis studies. The dashed lines represent the experimentally determined in vitro IC_{50} (free) of the three panRAF inhibitors against BRAF-mutant M12 melanoma cell line. Data represent mean ± S.D., n = 4.

JPET Fast Forward. Published on January 8, 2019 as DOI: 10.1124/jpet.118.253708
This article has not been copyedited and formatted. The final version may differ from this version.

Tables

Table 1. Physico-chemical properties of panRAF inhibitors.

	CCT196969	**LY3009120**	**MLN2480**
Molecular formula	$C_{27}H_{24}FN_7O_3$	$C_{23}H_{29}FN_6O$	$C_{17}H_{12}Cl_2F_3N_7O_2S$
Molecular weight (g/mol)	513.53	424.52	506.29
Solubility	< 1mg/mL	< 1mg/mL	< 1mg/mL
logP	5.5	4.2	3
logD (pH 7.4)	5.5	4.2	3
pKa[1]	10.36	11.61	10.29
Topological polar surface area (A^2)	123	92	136
Hydrogen bond donor count	3	3	3
Rotatable bond count	6	6	6

The reported properties were calculated using ChemAxon (http://www.chemicalize.com).
[1] The values represent strongest acidic pKa reported by ChemAxon

JPET Fast Forward. Published on January 8, 2019 as DOI: 10.1124/jpet.118.253708
This article has not been copyedited and formatted. The final version may differ from this version.

Table 2. Unbound fractions (fu) for CCT196969, LY3009120 and MLN2480 in plasma, brain and serum-containing cell culture media, determined by in vitro rapid equilibrium dialysis (RED) experiments. Data represent the mean ± S.D. (n = 3).

Inhibitor	Matrix	fu (%)
CCT196969	Plasma	0.1 ± 0.01
	Brain	0.50 ± 0.10
	Cell culture media	21.51 ± 1.58
LY3009120	Plasma	1.82 ± 0.18
	Brain	0.93 ± 0.04
	Cell culture media	27.90 ± 2.13
MLN2480	Plasma	4.21 ± 0.16
	Brain	0.98 ± 0.09
	Cell culture media	34.20 ± 1.52

fu, unbound (free) fraction

JPET Fast Forward. Published on January 8, 2019 as DOI: 10.1124/jpet.118.253708
This article has not been copyedited and formatted. The final version may differ from this version.

Table 3. Total and free (unbound) IC_{50} for vemurafenib (control) and panRAF inhibitors in patient derived melanoma cell lines (M12 and M27, BRAF-mutant; M15, NRAS-mutant). The free IC_{50} were estimated for the panRAF inhibitors using the total IC_{50} values and the unbound fractions (fu) in cell culture media.

	IC_{50} (μM) (95% confidence intervals)			**Free IC_{50} (μM)**		
	M12	**M27**	**M15**	**M12**	**M27**	**M15**
Vemurafenib	0.14 (0.10-0.19)	0.38 (0.28-0.52)	6.16 (4.94-7.68)	-	-	-
CCT196969	0.19 (0.13-0.27)	0.53 (0.41-0.70)	1.58 (1.21-2.07)	0.04	0.11	0.33
LY3009120	0.002 (0.001-0.003)	0.001 (0.07-0.002)	0.003 (0.001-0.008)	0.0006	0.0003	0.0008
MLN2480	3.59 (3.00-4.29)	3.83 (3.11-4.71)	7.71 (6.32-9.41)	1.22	1.30	2.62

JPET Fast Forward. Published on January 8, 2019 as DOI: 10.1124/jpet.118.253708
This article has not been copyedited and formatted. The final version may differ from this version.

Table 4. The pharmacokinetic/metric parameters of panRAF inhibitors in FVB wild-type mice following administration of single intravenous dose of 5 mg/kg. Data are presented as mean or mean ± S.E.M (n = 4).

	CCT196969		**LY3009120**		**MLN2480**	
	Plasma	**Brain**	**Plasma**	**Brain**	**Plasma**	**Brain**
Half-life (h)	2.79	3.37	2.35	1.74	6.54	7.25
$AUC_{(0-t)}$ (µg*h/mL)	150.23 ± 6.08	0.92 ± 0.02	10.86 ± 0.59	0.51 ± 0.03	17.56 ± 0.47	3.45 ± 0.09
$AUC_{(0-\infty)}$ (µg*h/mL)	155.07	0.97	10.88	0.51	22.71	4.49
CL (mL/min/kg)	0.54	-	7.66	-	3.7	-
Vd (L/kg)	0.13	-	1.56	-	2.08	-
Kp ($AUC_{(0-\infty)}$ ratio)	-	0.006	-	0.05	-	0.20
Kp,uu ($AUC_{(0-\infty)}$ ratio)	-	0.03	-	0.02	-	0.05

$AUC_{(0-t)}$, area under the curve from zero to the time of last measured concentration
$AUC_{(0-\infty)}$, area under the curve from zero to time infinity
CL, clearance
Vd, volume of distribution
Kp (AUC ratio), the ratio of $AUC_{(0-\infty,brain)}$ to $AUC_{(0-\infty,plasma)}$ using total drug concentrations
Kp,uu (AUC ratio), the ratio of $AUC_{(0-\infty,brain)}$ to $AUC_{(0-\infty,plasma)}$ using free drug concentrations

JPET Fast Forward. Published on January 8, 2019 as DOI: 10.1124/jpet.118.253708
This article has not been copyedited and formatted. The final version may differ from this version.

Table 5. The pharmacokinetic/metric parameters of CCT196969 and LY3009120 in FVB wild-type mice following administration of single oral dose. Data are presented as mean or mean ± S.E.M (n = 4).

	CCT196969 (10 mg/kg)		**LY3009120 (25 mg/kg)**	
	Plasma	**Brain**	**Plasma**	**Brain**
Half-life (h)	3.64	3.97	2.91	2.87
Tmax (h)	4	6	0.5	1
Cmax (µg/mL)	31.09 ± 7.15	0.40 ± 0.04	1.48 ± 1.01	0.04 ± 0.009
$AUC_{(0-t)}$ (µg*h/mL)	222.01 ± 18.94	2.18 ± 0.17	2.06 ± 0.44	0.09 ± 0.02
$AUC_{(0-\infty)}$ (µg*h/mL)	241.17	2.38	2.09	0.09
CL (mL/min/kg)	0.53	-	7.98	-
Vd (L/kg)	0.16	-	2.01	-
F (%)	77	-	4	-
Kp ($AUC_{(0-\infty)}$ ratio)	-	0.01	-	0.04
Kp,uu ($AUC_{(0-\infty)}$ ratio)	-	0.05	-	0.02

Tmax, time to reach the maximum concentration
Cmax, observed maximum concentration
$AUC_{(0-t)}$, area under the curve from zero to the time of last measured concentration
$AUC_{(0-\infty)}$, area under the curve from zero to time infinity
CL, clearance
Vd, volume of distribution
F (Absolute bioavailability), ratio of the dose corrected $AUC_{(0-\infty),po}$ to dose corrected $AUC_{(0-\infty),iv}$
Kp (AUC ratio), the ratio of $AUC_{(0-\infty,brain)}$ to $AUC_{(0-\infty,plasma)}$ using total drug concentrations
Kp,uu (AUC ratio), the ratio of $AUC_{(0-\infty,brain)}$ to $AUC_{(0-\infty,plasma)}$ using free drug concentrations

JPET Fast Forward. Published on January 8, 2019 as DOI: 10.1124/jpet.118.253708
This article has not been copyedited and formatted. The final version may differ from this version.

Table 6. Steady-state brain distribution of panRAF inhibitors in wild-type and *Mdr1a/b*$^{-/-}$ *Bcrp1*$^{-/-}$ mice. Data are presented as mean or mean ± S.D.

Inhibitor	Strain	Kp brain	Kp,uu brain	Distribution advantage
CCT196969	Wild-type	0.01 ± 0.002	0.05	1
	Mdr1a/b$^{-/-}$Bcrp1a/b$^{-/-}$	0.05 ± 0.02	0.25	5
LY3009120	Wild-type	0.01 ± 0.01	0.005	1
	Mdr1a/b$^{-/-}$Bcrp1a/b$^{-/-}$	0.27 ± 0.12	0.14	27
MLN2480	Wild-type	0.34 ± 0.10	0.08	1
	Mdr1a/b$^{-/-}$Bcrp1a/b$^{-/-}$	2.88 ± 0.31	0.66	8.5

Kp brain, the ratio of $C_{ss,brain}$ to $C_{ss,plasma}$ using total drug concentrations
Kp,uu brain, the ratio of $C_{ss,brain}$ to $C_{ss,plasma}$ using free drug concentrations
Distribution advantage, the ratio of Kp to $Kp_{wild-type}$

JPET Fast Forward. Published on January 8, 2019 as DOI: 10.1124/jpet.118.253708
This article has not been copyedited and formatted. The final version may differ from this version.

Table 7. Comparison of brain distribution of RAF inhibitors in wild-type mice. Data are presented as means.

Inhibitor	Intravenous dose (mg/kg)	Kp brain	Kp,uu brain
Vemurafenib[a]	2.5	0.004	NR
Dabrafenib[b]	2.5	0.02	NR
CCT196969	5	0.006	0.03
LY3009120	5	0.05	0.02
MLN2480	5	0.20	0.05

Kp (AUC ratio), the ratio of $AUC_{(0-\infty,brain)}$ to $AUC_{(0-\infty,plasma)}$ using total drug concentrations
Kp,uu (AUC ratio), the ratio of $AUC_{(0-\infty,brain)}$ to $AUC_{(0-\infty,plasma)}$ using free drug concentrations
NR, not reported
[a] As reported by Mittapalli et al. 2012
[b] As reported by Mittapalli et al. 2013

JPET Fast Forward. Published on January 8, 2019 as DOI: 10.1124/jpet.118.253708
This article has not been copyedited and formatted. The final version may differ from this version.

Figures

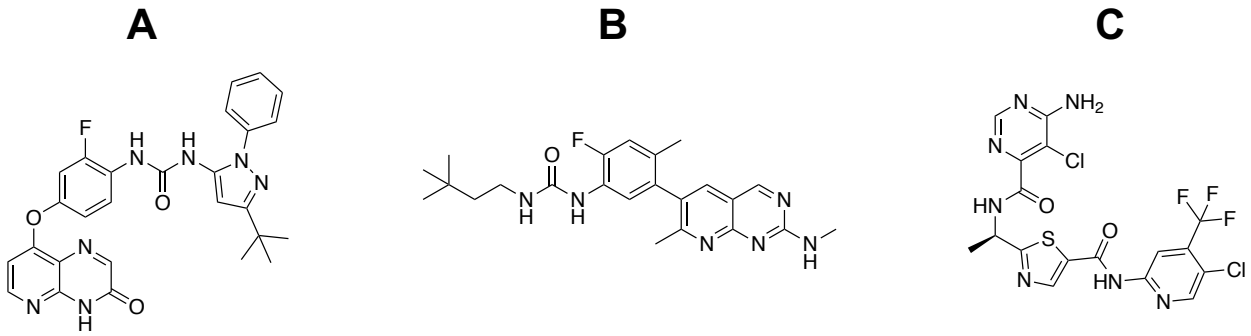

Fig 1.

JPET Fast Forward. Published on January 8, 2019 as DOI: 10.1124/jpet.118.253708
This article has not been copyedited and formatted. The final version may differ from this version.

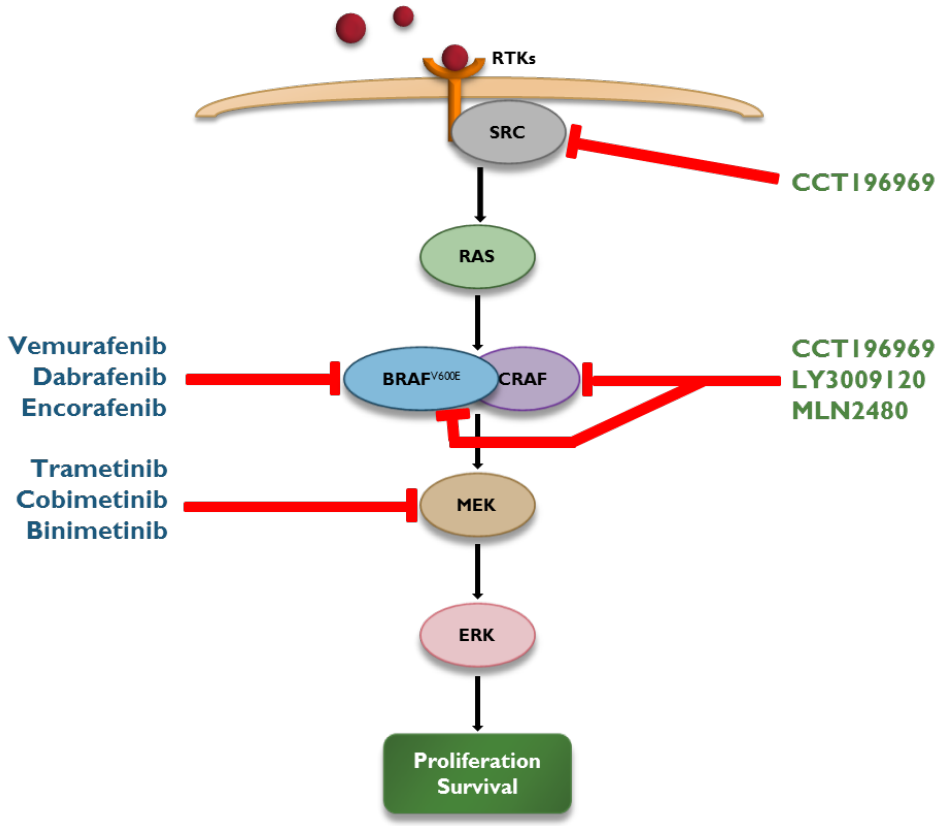

Fig 2.

JPET Fast Forward. Published on January 8, 2019 as DOI: 10.1124/jpet.118.253708
This article has not been copyedited and formatted. The final version may differ from this version.

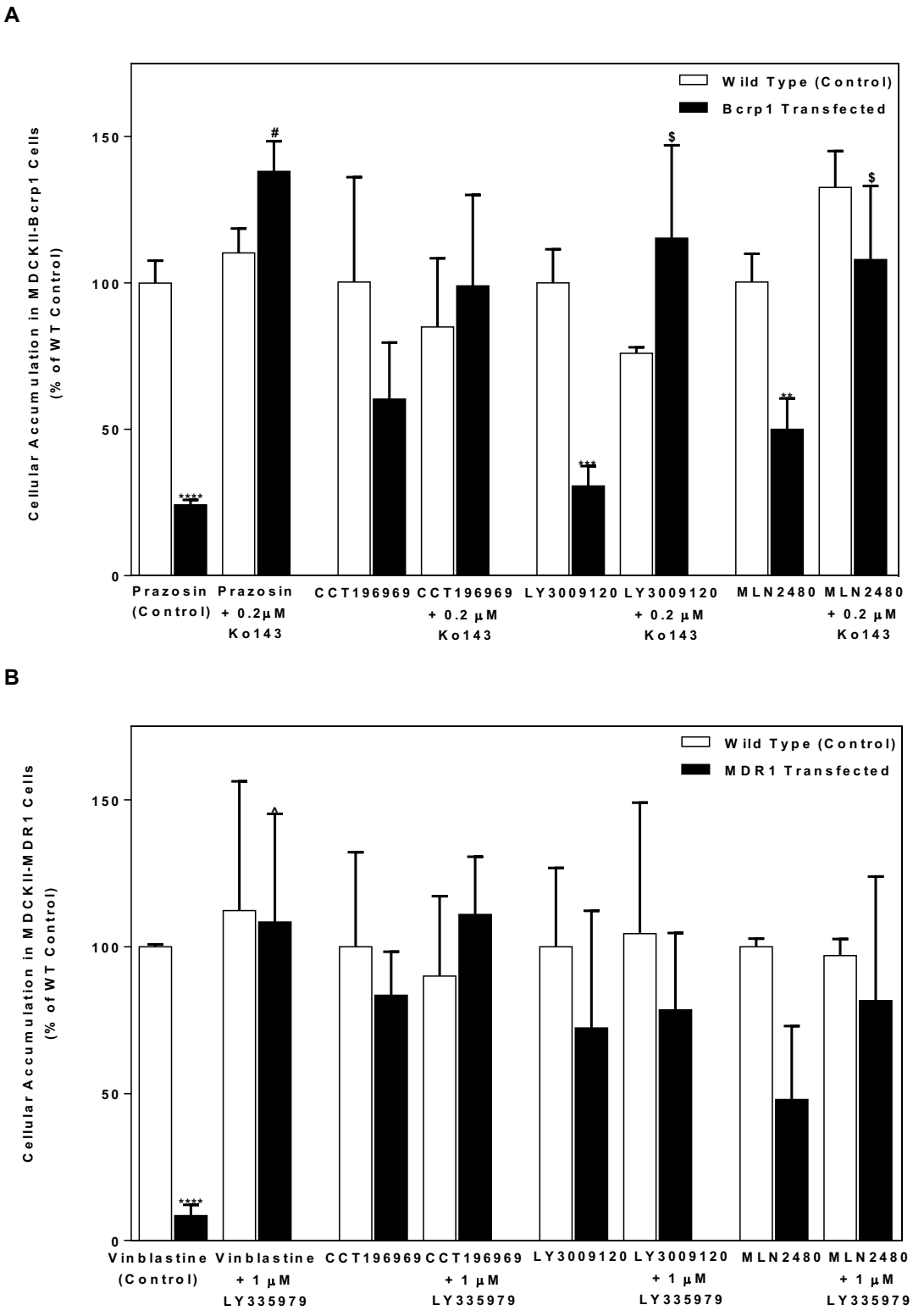

Fig 3.

JPET Fast Forward. Published on January 8, 2019 as DOI: 10.1124/jpet.118.253708
This article has not been copyedited and formatted. The final version may differ from this version.

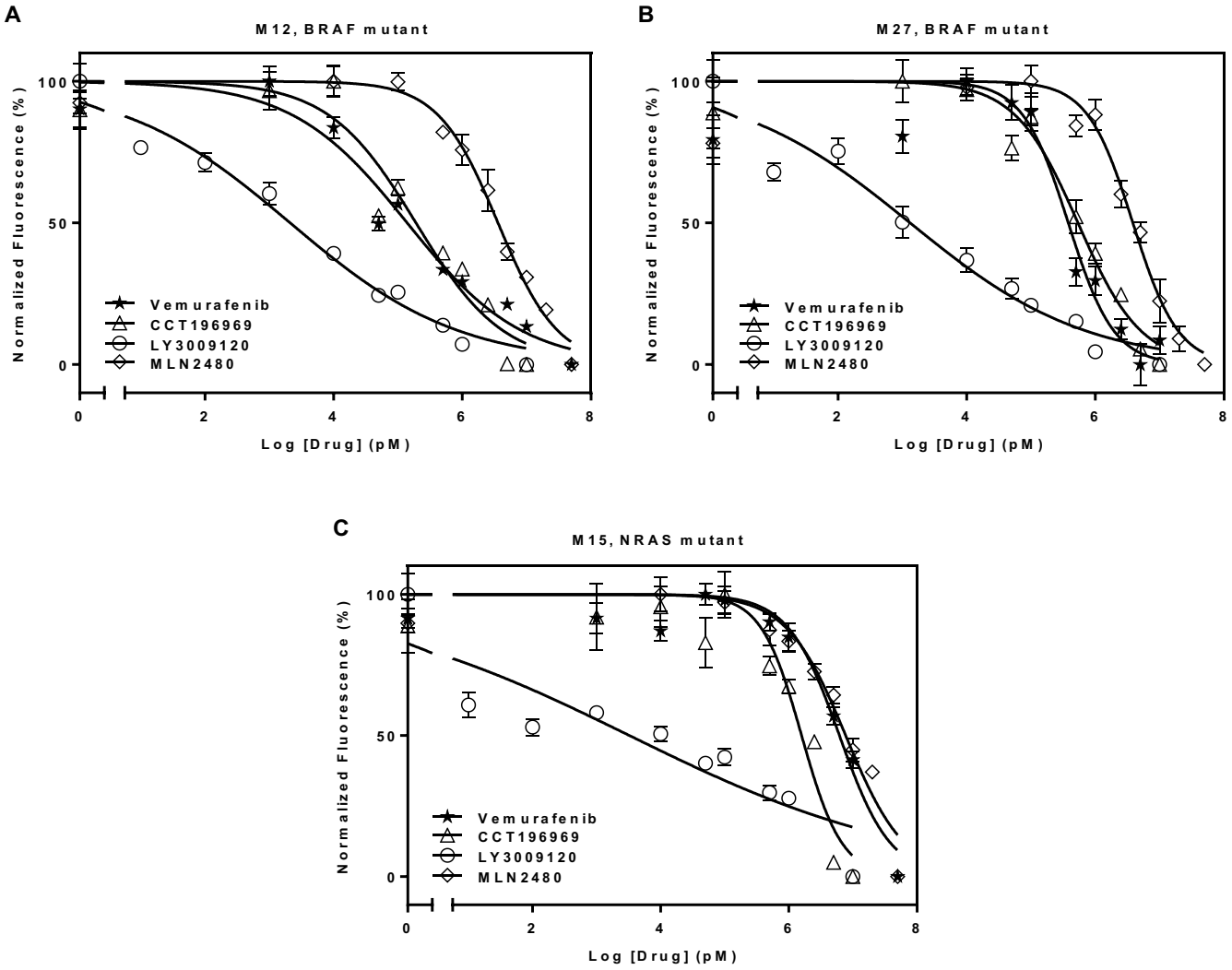

Fig 4.

JPET Fast Forward. Published on January 8, 2019 as DOI: 10.1124/jpet.118.253708
This article has not been copyedited and formatted. The final version may differ from this version.

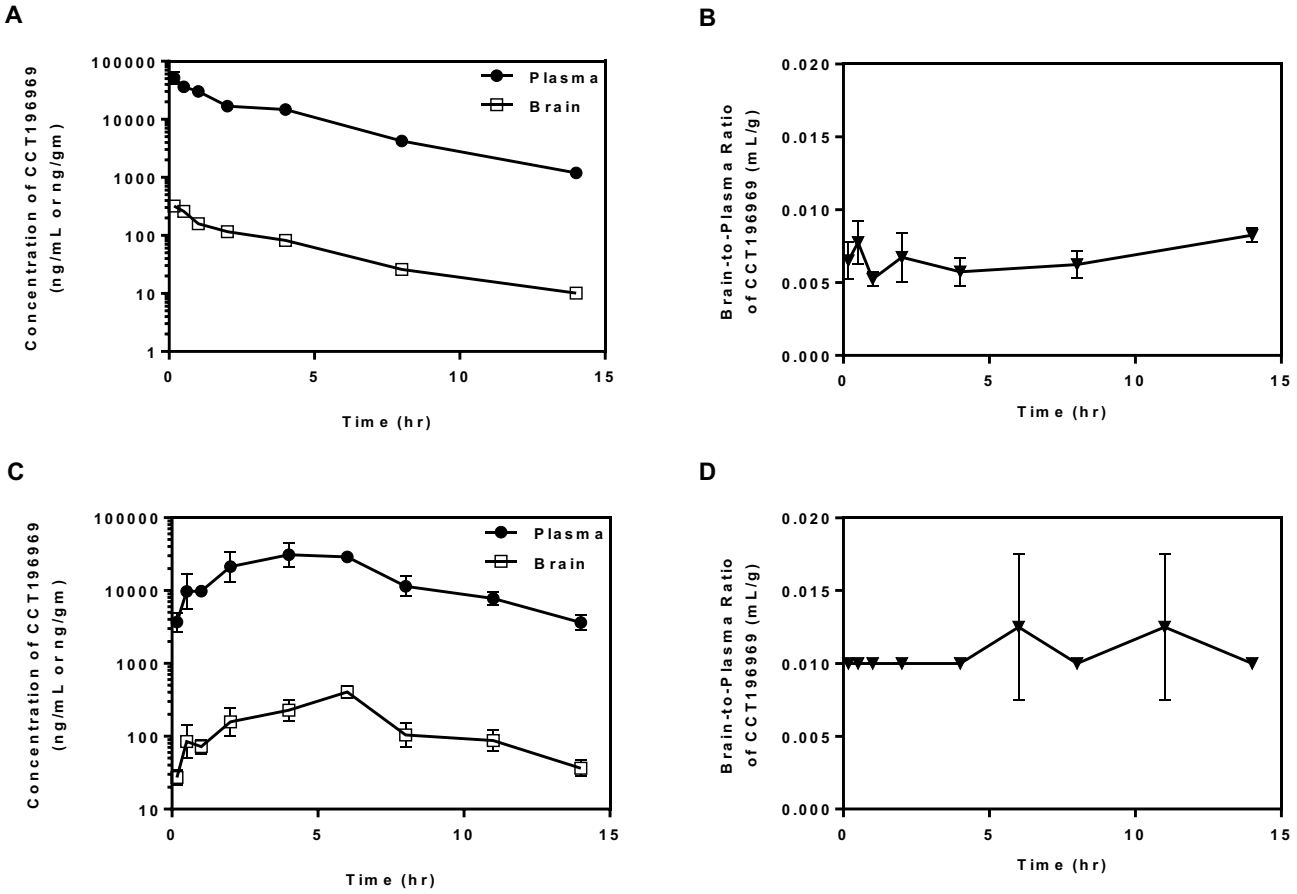

Fig 5.

JPET Fast Forward. Published on January 8, 2019 as DOI: 10.1124/jpet.118.253708
This article has not been copyedited and formatted. The final version may differ from this version.

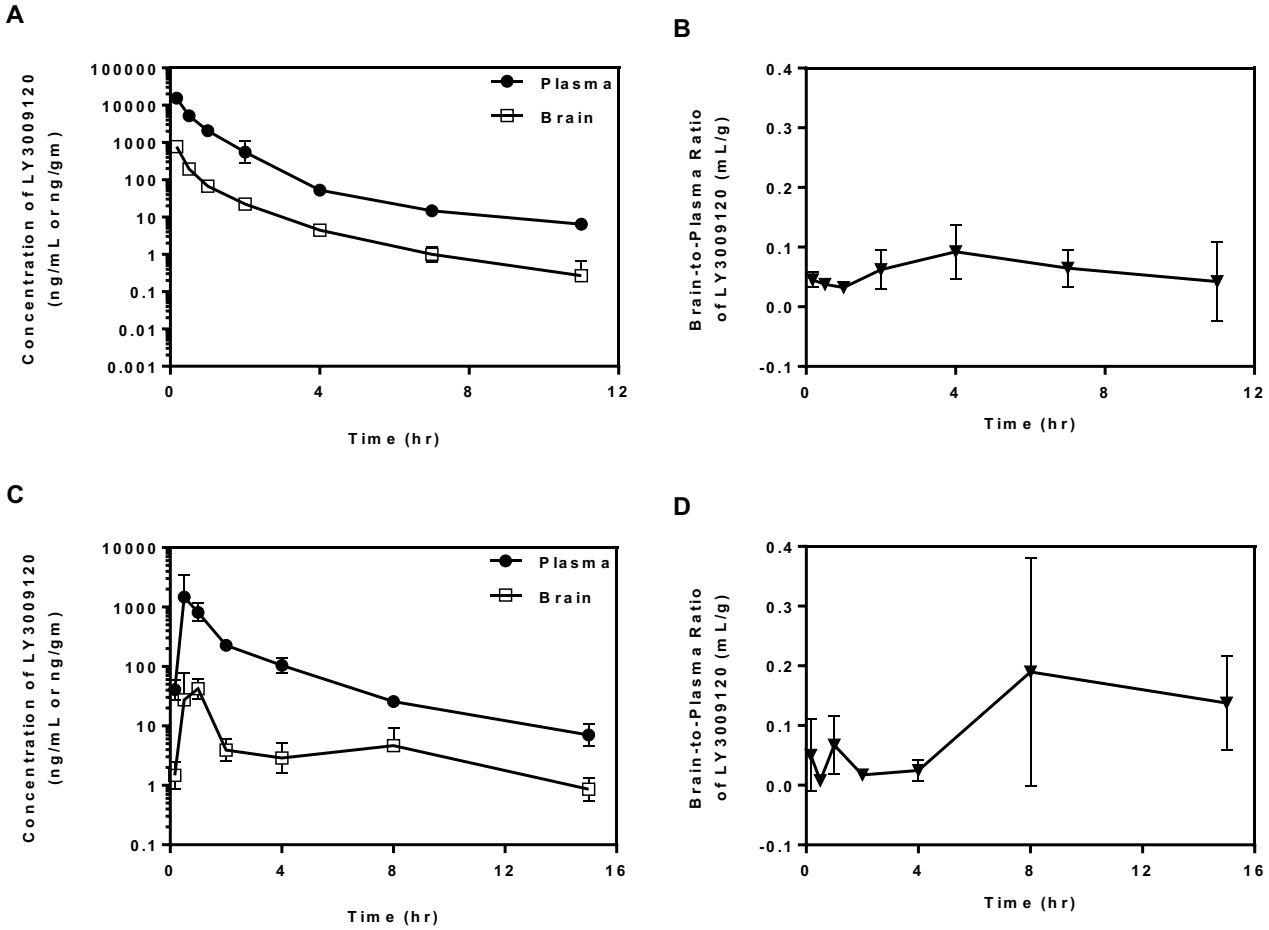

Fig 6.

JPET Fast Forward. Published on January 8, 2019 as DOI: 10.1124/jpet.118.253708
This article has not been copyedited and formatted. The final version may differ from this version.

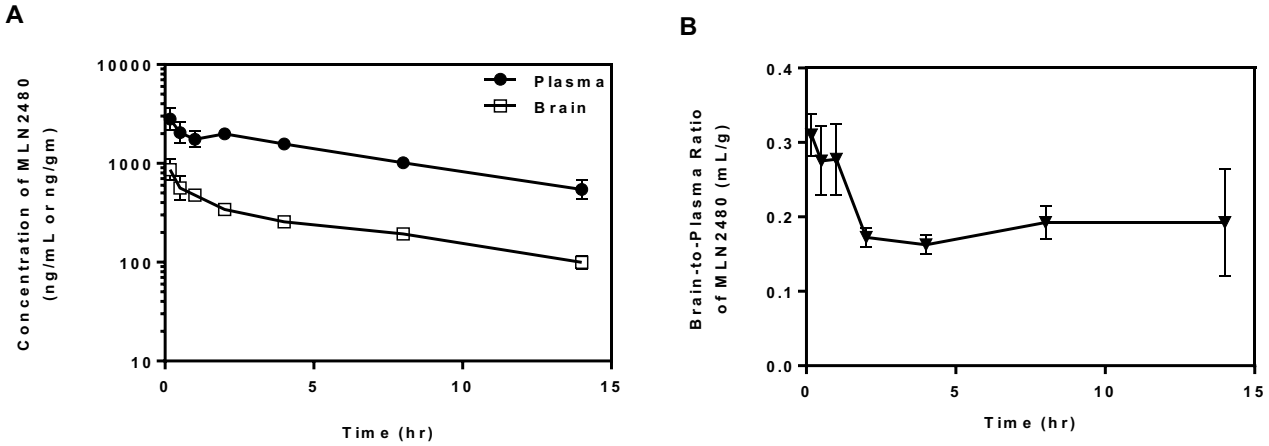

Fig 7.

JPET Fast Forward. Published on January 8, 2019 as DOI: 10.1124/jpet.118.253708
This article has not been copyedited and formatted. The final version may differ from this version.

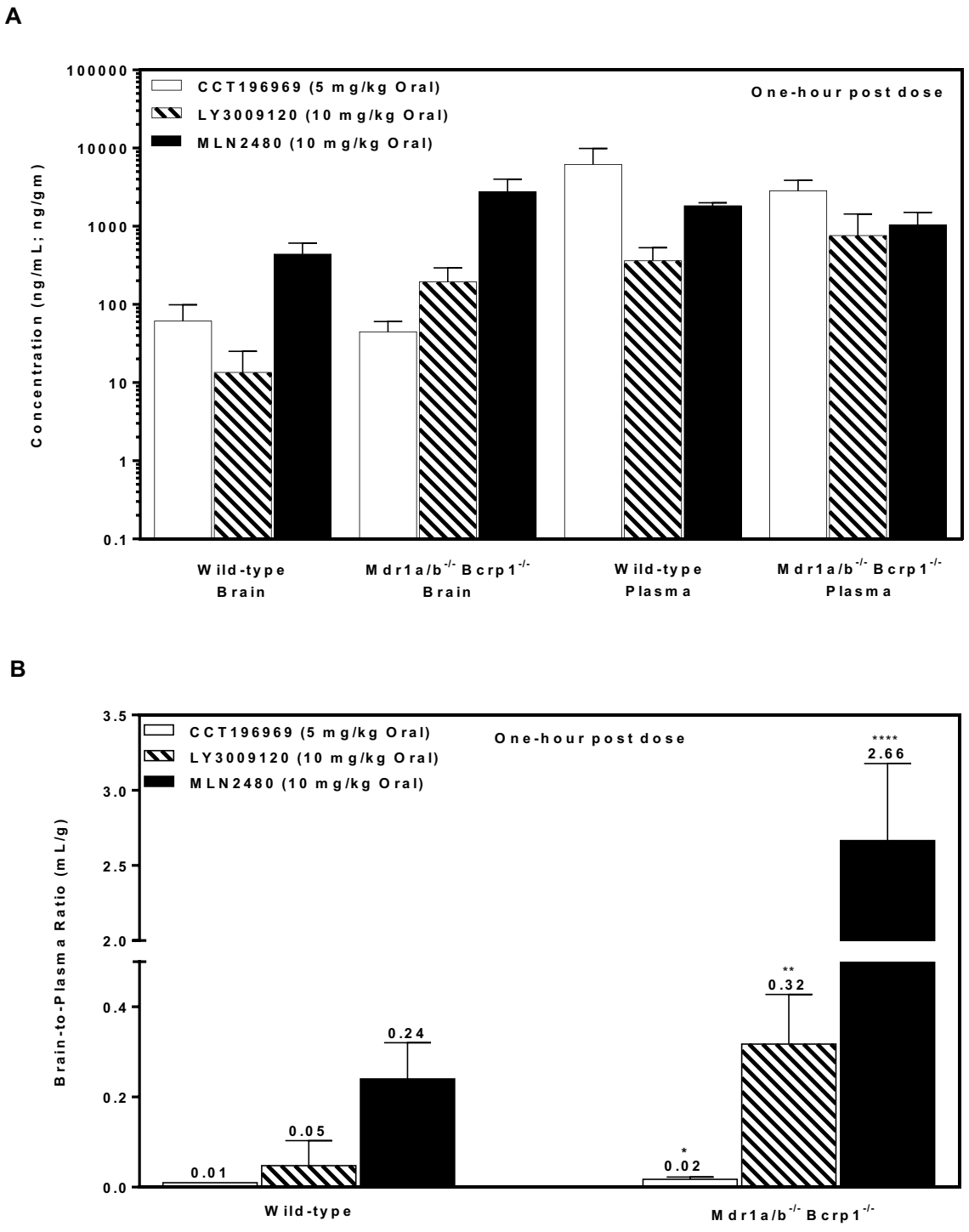

Fig 8.

JPET Fast Forward. Published on January 8, 2019 as DOI: 10.1124/jpet.118.253708
This article has not been copyedited and formatted. The final version may differ from this version.

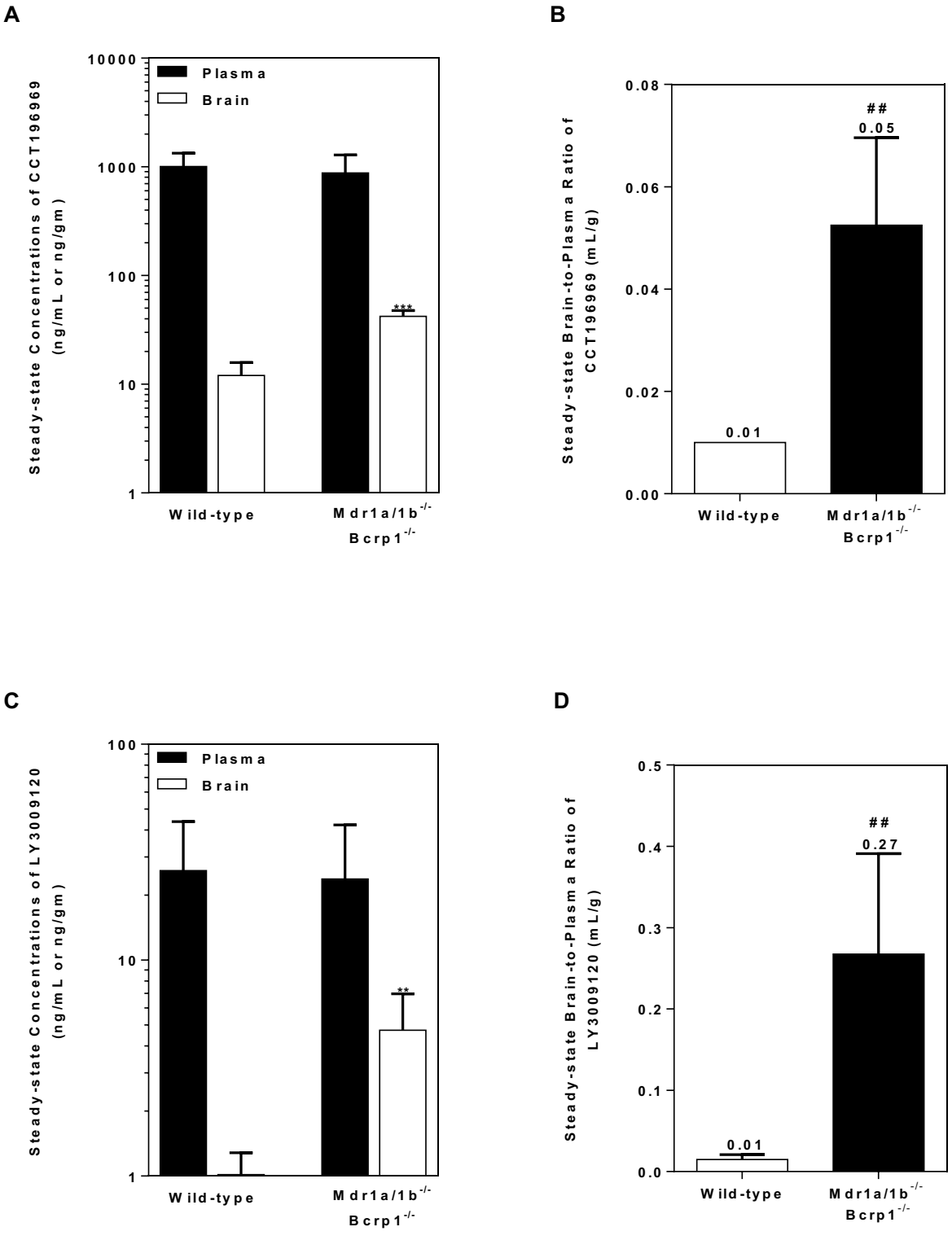

JPET Fast Forward. Published on January 8, 2019 as DOI: 10.1124/jpet.118.253708
This article has not been copyedited and formatted. The final version may differ from this version.

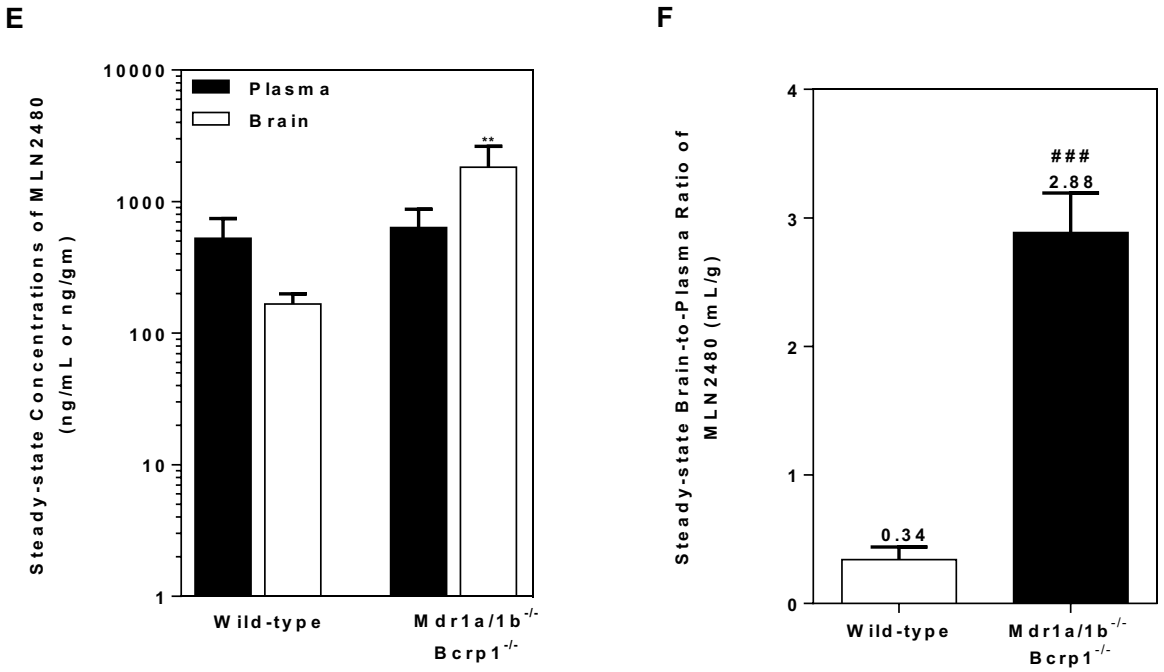

Fig 9.

JPET Fast Forward. Published on January 8, 2019 as DOI: 10.1124/jpet.118.253708
This article has not been copyedited and formatted. The final version may differ from this version.

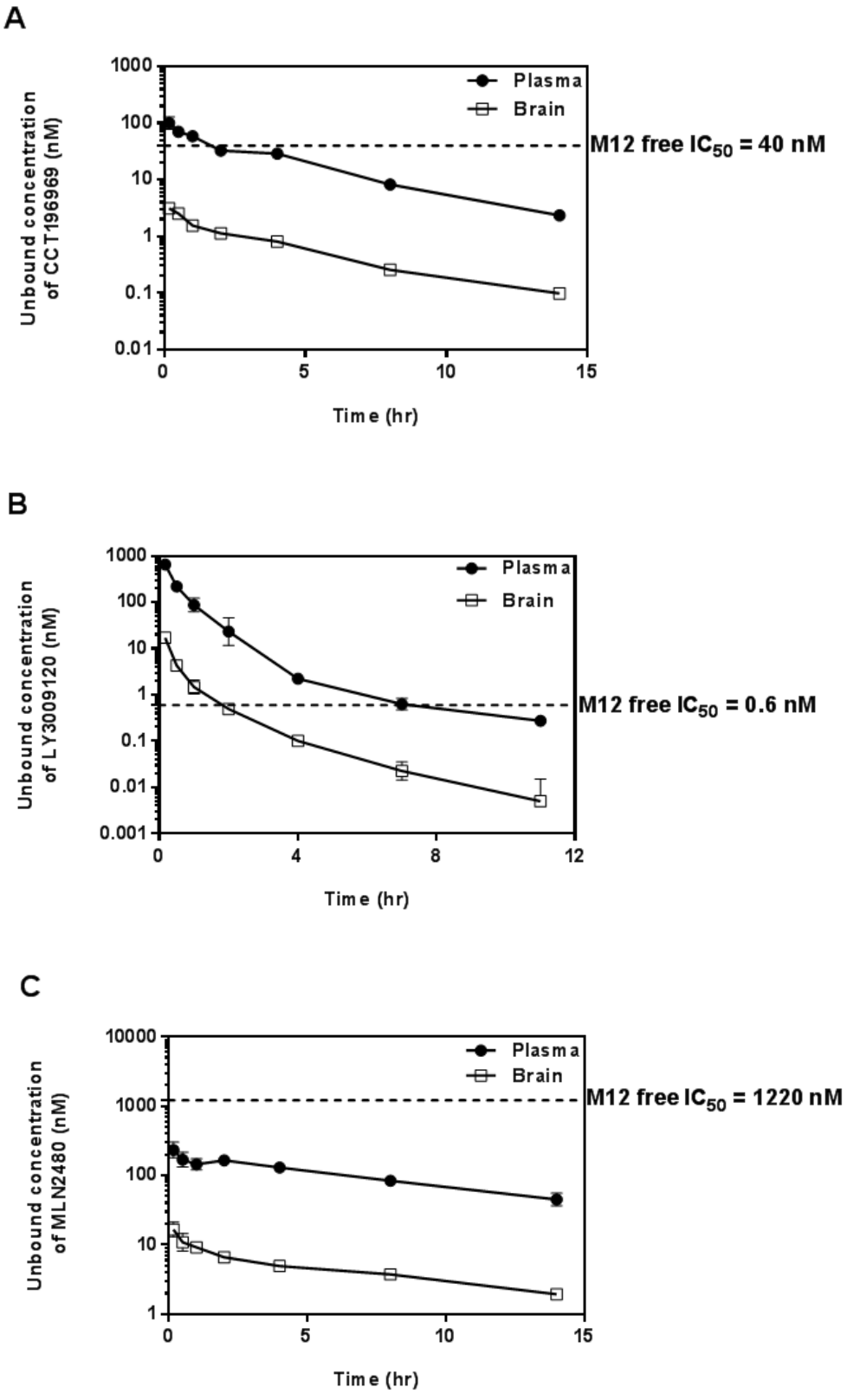

Fig 10.